Cell Reports

Article

Decoy antibodies block extracellular HSP70, prevent self-signaling, and inhibit melanoma cell survival

Graphical abstract

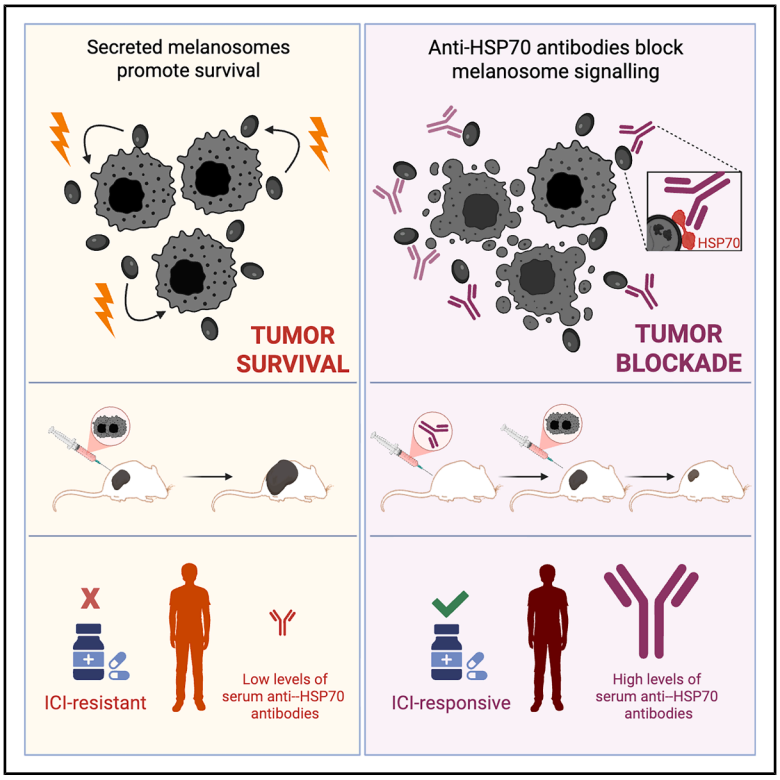

Authors

Noam Ben-Shalom, Shivang Parikh, Lilach Abramovitz, ..., Ronnie Shapira-Frommer, Carmit Levy, Natalia T. Freund

Correspondence

nfreund@tauex.tau.ac.il

In brief

Melanoma-derived melanosomes promote tumor survival. Ben-Shalom et al. demonstrate that melanosome immunization induces anti-HSP70 "decoy" antibodies that block this pro-survival signaling and suppress tumor growth. Similar antibody responses in patients correlate with clinical benefit, uncovering an extracellular vesicle-antibody axis with therapeutic and biomarker potential.

Highlights

- Melanoma-derived melanosomes function as protumorigenic autocrine survival units
- Immunization with melanosomes elicits protective anti-melanoma antibody responses
- Anti-melanosome mAbs target HSP70, block it, and inhibit melanoma growth
- Patients with complete response to therapy have elevated anti-HSP70 antibody titers

Ben-Shalom et al., 2026, Cell Reports *45*, 117300
May 26, 2026
https://doi.org/10.1016/j.celrep.2026.117300

CellPress

Cell Reports

CellPress
OPEN ACCESS

Article

Decoy antibodies block extracellular HSP70, prevent self-signaling, and inhibit melanoma cell survival

Noam Ben-Shalom,[1,2] Shivang Parikh,[1] Lilach Abramovitz,[1] Ron Yefet,[1] Paulee Manich,[1] Dafna Tussia-Cohen,[3] Ori Moskowitz,[1] Roma Parikh,[1] Stav Melamed,[1] Ksenia Polonsky,[3] Sebastien Apcher,[4] Tzachi Hagai,[3] Merav Cohen,[1] Yochai Wolf,[5,6] Ronnie Shapira-Frommer,[5] Carmit Levy,[1] and Natalia T. Freund[1,7,*]

[1]Gray School of Medical Sciences, Gray Faculty of Medical & Health Sciences, Tel Aviv University, Tel Aviv 6997801, Israel
[2]Department of Pathology and Immunology, Washington University School of Medicine, St Louis, MO 63110, USA
[3]Shmunis School of Biomedicine and Cancer Research, George S Wise Faculty of Life Sciences, Tel Aviv University, Tel Aviv 69978, Israel
[4]Gustave Roussy Cancer, Campus, INSERM U1015, Universite Paris-Saclay, 114 rue, Edouard Vaillant, 94800 Villejuif, France
[5]Sheba Medical Center, Ramat Gan 52621, Israel
[6]Department of Pathology, Gray Faculty of Medical & Health Sciences, Tel Aviv University, Tel Aviv 6997801, Israel
[7]Lead contact
*Correspondence: nfreund@tauex.tau.ac.il
https://doi.org/10.1016/j.celrep.2026.117300

SUMMARY

Melanoma cells secrete melanosomes, large extracellular vesicles that reinforce tumor growth and survival signaling. To determine whether these vesicles elicit functional humoral immunity, we immunized mice with melanoma-derived melanosomes and analyzed the resulting antibody responses. This approach induced B cell expansion and generated antibodies directed against heat shock protein 70 (HSP70) present on the surface of melanosomes. Functionally, anti-HSP70 monoclonal antibodies inhibited growth in murine B16 and human MNT-1 melanoma cells independently of immune effector cells while suppressing key transcriptional programs involved in proliferation. *In vivo*, passive administration of anti-HSP70 antibodies delayed tumor onset and improved survival in a prophylactic B16 model. Moreover, in patients with metastatic melanoma treated with immune checkpoint blockade, higher serum anti-HSP70 immunoglobulin G (IgG) levels were associated with complete response compared with progressive disease. Together, these findings identify an extracellular vesicle-antibody axis that constrains melanoma survival signaling and has biomarker and therapeutic implications.

INTRODUCTION

Melanoma is the most lethal of human skin cancers, accounting for the majority of skin-cancer-related deaths, even though it comprises only a small percentage of all skin cancer cases.[1–3] Despite remarkable progress in therapy, including targeted treatments and immunotherapies, many patients develop resistance to these treatments over time.[4–8] Approximately 50% of patients with BRAF-mutated melanoma relapse within 1 year of starting combined BRAF/MEK inhibitor therapy.[9] Additionally, a significant proportion of patients fail to respond to immune checkpoint inhibitors or experience only transient benefits before disease progression.[10] Thus, a breakthrough in developing new strategies to prevent melanoma recurrence and metastasis is essential to overcoming treatment resistance and improving long-term outcomes for patients with advanced melanoma.

Immune response plays a crucial role in melanoma.[11,12] Despite substantial evidence supporting T cells as key mediators of anti-melanoma immunity, either by directly killing tumor cells or activating other immune cells,[13–15] the role of B cells in tumor response and surveillance remains less understood.[16–18] Studies suggest that tumor-infiltrating B cells are associated with improved survival[19–22] and enhanced responsiveness to immunotherapy.[23,24] Furthermore, patients with melanoma exhibit antibody responses, particularly autoantibodies against intracellular antigens such as tubulin, YWHAZ, MASP1, H4C1, and PF4, which are elevated in active disease.[25] Notably, Fässler M. et al. demonstrated that higher antibody titers against melanocyte differentiation antigens (TRP1, TRP2, gp100, and MelanA/MART1) correlated with improved responses to immune checkpoint inhibitors, prolonged progression-free intervals, and better overall survival.[26] Similarly, Stockert et al. reported that 9.4% of patients with melanoma exhibited antibody responses against the cancer-testis antigen NY-ESO-1, a biomarker linked to improved survival.[27] However, these antibodies have primarily been investigated as diagnostic markers, and their functional role in melanoma immunity remains unclear.

Melanoma progression is characterized by the secretion of melanosomes by melanoma cells.[28] Melanosomes are specialized extracellular vesicles (EVs), 200–500 nm in size, produced

by melanocytes and primarily responsible for melanin transport.[29] In cancer, melanosomes are reprogrammed to carry cancer-associated factors[30] and microRNAs that drive phenotypic changes in the tumor microenvironment, particularly in cancer-associated fibroblasts (CAFs) and stromal cells, thereby promoting tumor progression.[28,31–33] Melanosomes are implicated in worsening disease outcomes[34] and contribute to drug resistance.[35] Although melanoma-derived melanosomes are large and enriched with cancer-associated proteins, they are restricted to the tissue, and their potential immunogenicity and the characteristics of antibodies targeting them have never been investigated.

In this study, we demonstrate for the first time that intravenous injection of melanoma-derived melanosomes into mice elicits protective B cell and antibody responses directed against the extracellular form of heat shock protein 70 (HSP70), a family of key regulators that promote self-signaling and proliferation of melanoma. Antibodies targeting this extracellular form of HSP70 inhibit melanoma cell growth, independently of additional immune effectors. Remarkably, we find that anti-HSP70 serum antibodies are naturally produced in patients with melanoma, which correlate with better response to immunotherapy. Our study unlocks the immunogenic potential of melanoma-derived melanosomes as a platform for melanoma vaccine, opening new promising avenues for therapeutic intervention.

RESULTS

Melanosome immunization promotes protection against melanoma in mice

Melanosomes are secreted into the surrounding tissues via a paracrine mechanism.[36] To test whether melanoma melanosomes are immunogenic when administered systemically, we isolated melanosomes from B16 murine melanoma cell line[37] (see Materials and Methods) and immunized C57BL/6 mice (n = 9) intravenously three times with melanosomes (Figure 1A). Nineteen days following Boost 2, we subcutaneously challenged the mice with 100,000 B16 melanoma cells. Mice immunized with melanosomes exhibited significantly prolonged survival compared to PBS control (p = 0.0019), with 33% of immunized mice surviving until the end of the experiment (day 70), whereas none in the control group did (Figure 1B). Tumor onset in melanosome-immunized mice was delayed (average day 30 versus day 10 in controls), and tumors that did develop were smaller (Figures 1C and 1D). Serological analysis by ELISA revealed increasing production of melanosome-specific immunoglobulin G (IgG) (Figure 1E). Consistently, melanosome immunization induced a 3.6-fold increase in germinal center (GC) B cells (Figures 1F and 1G) and significant increases in $CD4^+$ (1.5-fold) and $CD8^+$ T cells (1.3-fold; Figures 1H and 1I), while natural killer (NK) cells remained unchanged (Figure S1).

Anti-melanosome mAbs block melanosome signaling and inhibit growth

We investigated whether antibodies directed against melanosomes can mediate tumor suppressive functions and inhibit melanoma growth. Sera from melanosome-immunized mice (n = 10) were collected on days 3, 5, 8, 10, 12, and 14 (Figure 2A). Anti-melanosome IgG became detectable by ELISA starting from day 8 post-immunization and continued to increase over time (Figure 2B). This binding was no longer detected when the melanosomes were trypsinized, indicating that the antibodies target membrane-associated proteins on the surface of melanosomes (Figure S2). Next, we single-cell sorted IgG^+ GC B cells from spleens of four mice (Figures 2C and 2D), followed by IgH and IgK amplification and sequencing, as previously described[38,39] (Table S1). All mice exhibited expanded B cell clones, showing progressive accumulation of somatic hypermutations (SHMs) and clonal bursts (Figures 2E and S3). We produced 13 monoclonal antibodies (mAbs), representing the different expanded B cell clonal families. Most mAbs exhibited binding to purified B16 melanosomes, as detected by ELISA and flow cytometry (Figures 2F and 2G). Among the mAbs tested, Mel321-31, Mel322-34, and Mel321-35 exhibited the strongest binding and were therefore selected for further studies.

Purified B16 melanosomes had a striking effect on B16 melanoma cells, markedly increasing fluorescence intensity by promoting greater cell adherence. Within just 2 h of culture, cells exposed to melanosomes exhibited a 148% increase in intensity compared to untreated controls (Figure 2H, black vs. empty circles). While melanosomes have previously been shown to support the growth of fibroblasts and tumor-associated stromal cells, our findings reveal that they also enhance the proliferation of the melanoma cells that secrete them. This autocrine-like "melanosomal effect" was abolished when melanosomes were pre-incubated with monoclonal antibodies Mel322-34 or Mel321-35 (Figures 2H and S4). Partial inhibition was observed with Mel321-31. These results indicate that melanosome-targeting antibodies are acting as decoys that block the melanosomal growth-promoting effects.

Anti-melanosome mAbs inhibit B16 melanoma cell survival

MAbs Mel321-31, Mel322-34, and Mel321-35 significantly impaired the growth of TdT-expressing B16 melanoma cells over 60 h, reducing cell growth by 4.1-, 8.4-, and 8.2-fold, respectively, relative to the isotype control, as quantified by B16 fluorescence intensity (Figures 3A and S5). Incubation of B16 cells with melanosome-targeting mAbs increased caspase-3/-7 activity detected using an activated fluorescent DNA dye, suggesting that the mAbs induced apoptosis (Figure 3B). To further explore this, we performed mRNA sequencing analysis. We identified 23 significantly downregulated genes shared among B16 cells treated with Mel321-31, Mel322-34, and Mel321-35 versus cells cultured with isotype control. Among these, 12 were related to apoptosis and survival, 5 to cytoskeleton organization, 3 to metabolism, and 3 to stress response (see Materials and Methods; Figure 3C). Gene set enrichment analysis (GSEA) identified only significantly downregulated pathways in mAb-treated cells. Notably, the interleukin 6 (IL-6)/Janus kinase (JAK)/signal transducer and activator of transcription 3 (STAT3) signaling pathway was consistently and significantly suppressed across all three mAbs (Figure 3D). This pathway plays a critical role in tumor cell proliferation, survival, invasion, and metastasis.[41] Reduction in IL-6 following mAb treatment

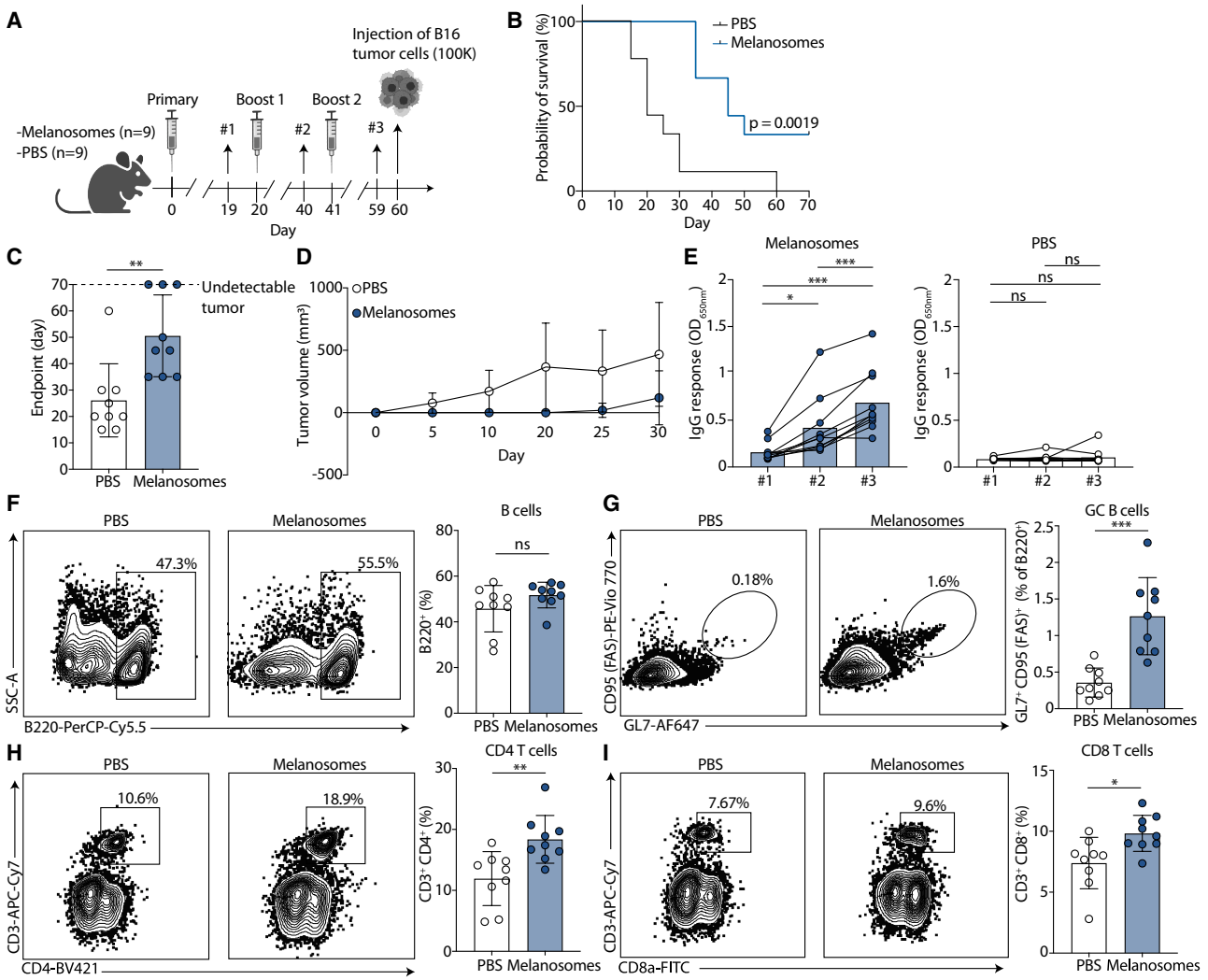

Figure 1. Melanosome immunization promotes improved survival following melanoma-challenge

(A) Schematic representation of the melanosome immunization and melanoma challenge protocol. C57BL/6 mice were immunized with 1 μg melanosomes or PBS on day 0, followed by booster immunizations with 10 μg of melanosomes or PBS on days 20 and 41. On day 60, mice were challenged with a subcutaneous injection of 100,000 B16 melanoma cells. Blood samples were collected on days 19, 40, and 59 (n = 9 per group).

(B) Kaplan-Meier survival curves comparing melanosome-immunized mice (blue, n = 9) and PBS-immunized mice (black, n = 9) after B16 melanoma challenge; the experiment was repeated two times.

(C) Endpoint day for each mouse. Time to reach the tumor growth limit for individual mice in groups immunized with melanosomes (n = 9) and PBS (n = 9).

(D) Tumor volume quantification (in mm^3) over time in melanosome-immunized (blue circles, n = 9) and PBS-immunized (white circles, n = 9) mice. Tumor volume was calculated as follows: $V = 0.5 \times \text{length} \times \text{width}^2$.

(E) Serum IgG responses to melanosomes in melanosome-immunized mice (left, n = 9) and in PBS-immunized controls (right, n = 9); as measured by ELISA, presenting the raw $O.D.650_{nm}$ at three time points: day 19 (#1), day 40 (#2), and day 59 (#3); the experiment was repeated three times.

(F–I) Flow cytometry plots of cell populations in the spleens of one representative melanosome-immunized and PBS-immunized mouse. The frequencies of the gated populations of all (n = 9) mice in each group are presented in the right panels. The immune populations include (F) B cells ($B220^+$), (G) GC B cells [$B220^+$ CD95 $(FAS)^+$ $GL7^+$], (H) $CD4^+$ T cells ($CD3^+$ $CD4^+$), and (I) $CD8^+$ T cells ($CD3^+$ $CD8^+$). The experiment was repeated two times. Graphs in (C), (D), and (F–I) present the mean ± SD, with each symbol representing an individual mouse. Graphs in (E) present the mean, with each symbol representing an individual mouse. Statistical significance was determined using GraphPad Prism by log rank (Mantel-Cox) test in (B), Mann-Whitney U test in (C), repeated measures one-way ANOVA with Tukey's multiple comparisons test in (E), and unpaired two-sided Welch's t test in (F–I). $^*p < 0.05$, $^{**}p < 0.01$, $^{***}p < 0.001$, $^{****}p < 0.0001$; "ns" indicates non-statistically significant differences.

was confirmed by ELISA, although for Mel321-31 the reduction in IL-6 did not reach statistical significance (Figure 3E). These results support the observation that Mel321-31, Mel322-34, and Mel321-35 change the cellular transcriptional landscape.

Anti-melanosome mAbs prolong survival in B16-challenged mice

To estimate the ability of the mAbs to inhibit tumor development *in vivo*, we administered 70 μg of antibody (Mel321-31,

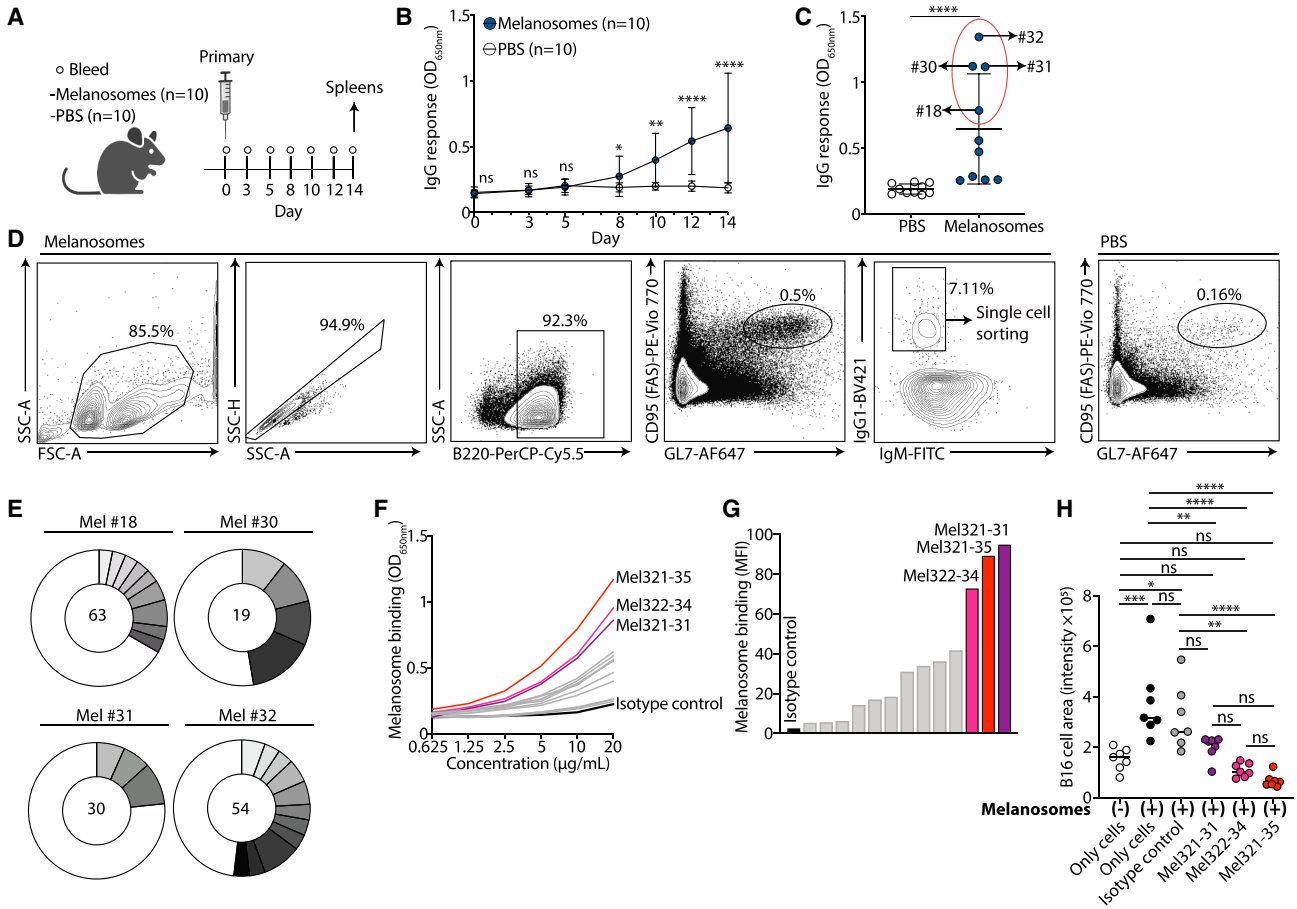

Figure 2. Melanosome-immunized mice show a profound B cell clonal expansion

(A) Schematic representation of the melanosome-immunization protocol. C57BL/6 mice (n = 10 per group) were immunized with 10 μg of melanosomes or PBS, and blood was collected on days 0, 3, 5, 8, 10, 12, and 14 following immunization. Spleens were harvested on day 14 post-immunization.

(B) Serum IgG response to melanosomes, measured by ELISA, in melanosome-immunized and PBS-immunized mice (n = 10 per group). Group mean raw O.D. 650 nm values at each time point (days 0, 3, 5, 8, 10, 12, and 14); the experiment was repeated three times.

(C) Serum IgG response to melanosomes, measured by ELISA, in individual melanosome-immunized and PBS-immunized mice (n = 10 per group) on day 14 post-immunization. The raw O.D. 650 nm values are presented. The four melanosome-immunized mice that were selected for B cell sorting (#18, #30, #31, and #32) are indicated by a red oval; the experiment was repeated three times.

(D) Left: representative flow cytometry plot and gating strategy of IgG1$^+$ GC B cells from a spleen of a melanosome-immunized mouse. The population that was single-cell sorted is indicated. Gating: lymphocytes → single cells → B cells (B220$^+$) → GC B cells (CD95 (FAS)$^+$ GL7$^+$) → IgG1$^+$ (IgG1$^+$ IgM$^-$). Right: GC B cells [CD95 (FAS)$^+$ GL7+] staining from a spleen of a PBS-immunized mouse.

(E) Pie charts showing the number of paired IgG1$^+$ Kappa sequences from the four melanosome-immunized mice (#18, #30, #31, and #32). The total number of sequences from each mouse is displayed in the center of each pie. Shaded slices indicate expanded B cell clones, while white slices represent unique sequences.

(F) Binding of mAbs to melanosomes (n = 13, 10 μg/mL), assessed by ELISA (the y axis shows raw O.D. 650 nm values). mGO.53.53 (black line) serves as an isotype control.[40] The three highest binding mAbs Mel321-31, Mel322-34, and Mel321-35 are depicted in purple, magenta, and red, respectively, while the other 10 mAbs are in gray.

(G) Binding of mAbs to melanosomes (2.5 μg/mL), as measured by flow cytometry (n = 13 mAbs, 10 μg/mL) and detected by staining with anti-mouse IgG conjugated to Alexa Fluor 647. Median fluorescence intensity (MFI, y axis) was calculated for each mAb. The three highest binding mAbs Mel321-31, Mel322-34, and Mel321-35 are depicted in purple, magenta, and red, respectively, while the other 10 mAbs are in gray. mGO.53 is in black and serves as an isotype control; the experiment was repeated three times.

(H) Quantification of fluorescence intensity of TdT-expressing B16 cells under different treatment conditions: untreated cells (no melanosomes, white circles), cells with 5 μg/mL of external melanosomes (black circles), cells treated with isotype control, mGO.53 (25 μg/mL) plus 5 μg/mL of external melanosomes (gray circles), Mel321-31 (25 μg/mL) plus 5 μg/mL of external melanosomes (purple circles), Mel322-34 (25 μg/mL) plus 5 μg/mL of external melanosomes (pink circles), and Mel321-35 (25 μg/mL) plus 5 μg/mL of external melanosomes (red circles). n = 7 per treatment group; the experiment was repeated three times. Data are presented as linear fluorescence values. Graphs (B) and (C) present the mean ± SD, with each symbol representing an individual mouse. Statistical significance was determined using GraphPad Prism by Mann-Whitney U test in (B) and (C) and by one-way ANOVA with Tukey's multiple comparisons post-test in (H). *p < 0.05, **p < 0.01, ***p < 0.001, ****p < 0.0001; "ns" indicates non-statistically significant differences.

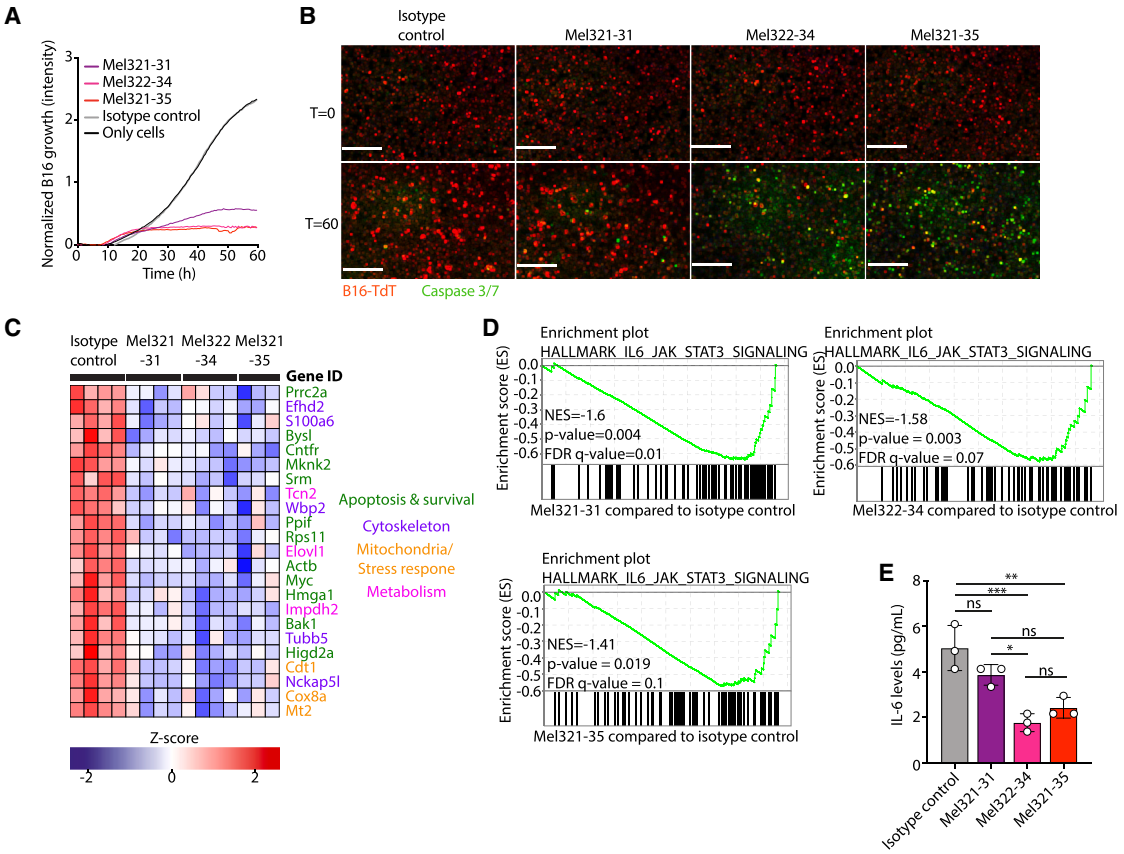

Figure 3. Anti-melanosome mAbs inhibit melanoma cell growth

(A) Quantification intensity of 15 × 10^3 TdT-expressing B16 cells over 60 h following treatment with mAbs (25 μg/mL, six repeats for each mAb), measured by IncuCyte. No mAb ("only cells," black) and mGO.53 (isotype control, gray) serve as controls. The three mAbs Mel321-31, Mel322-34, and Mel321-35 are depicted in purple, magenta, and red, respectively. The experiment was repeated three times.

(B) Representative images of TdT-expressing B16 cells (red) merged with caspase-3/-7-activated cells (green) at 0 and 60 h post-treatment. Scale bars: 400 μm.

(C) Heatmap showing z-scaled log-normalized counts per million for shared downregulated differentially expressed genes in B16 cells after 24-h treatment with mAbs Mel321-31 (n = 4), Mel322-34 (n = 4), and Mel321-35 (n = 3) and isotype control, mGO.53 (n = 4).

(D) GSEA of downregulated pathways shared among B16 cells following 24-h treatment with mAbs Mel321-31, Mel322-34, and Mel321-35 compared to isotype control, mGO.53.

(E) IL-6 quantification by ELISA. mAbs (25 μg/mL)—Mel321-31 (n = 3), Mel322-34 (n = 3), Mel321-35 (n = 3), and mGO.53 (n = 3)—were incubated with B16 cells. The supernatant was collected after 40 h and analyzed for IL-6 levels; n = 3, the experiment was repeated two times. Graph (E) presents the mean ± SD, with each symbol representing an individual replicate. Statistical significance was determined using GraphPad Prism by one-way ANOVA with Tukey's multiple comparisons post-test in (E). *p < 0.05, **p < 0.01, ***p < 0.001; "ns" indicates non-statistically significant differences.

n = 10; Mel322-34, n = 10; Mel321-35, n = 10) or the isotype control (n = 10) intraperitoneally to C57BL/6 mice 1 h before injecting subcutaneously 100,000 B16 melanoma cells. A second dose of 35 μg mAb was administered 1 week after tumor injection, and the mice were monitored for tumor growth and survival (Figure 4A). Mice treated with Mel322-34 and Mel321-35 showed a significant increase in survival (27% increase and 48% increase, respectively), compared to mice treated with isotype control. Mice treated with Mel321-31 had similar survival rates to mice treated with isotype control (Figure 4B). Notably, treatment with Mel321-35 also led to a significant delay in tumor onset in the mice (average of 15.5 days in isotype control compared to average of 22.9 days in Mel321-35; Figure 4C). The mAbs reduced tumor volume and inhibited tumor growth compared to mice treated with isotype control (Figures 4D and 4E). Focusing on Mel321-35, which conferred the strongest survival benefit, we found no major differences in splenic macrophage, NK cell, or $CD4^+$ and $CD8^+$ T cell frequencies (Figures S6A–S6D). In contrast, the melanosome-targeting mAb reduced splenic B cell frequencies (Figure 4F). This reduction was accompanied by an increase in activated B cells ($B220^+$ $CD69^+$) within the tumor-draining lymph node (TDLN) relative to controls, without changes in overall tumor immune infiltration ($CD45^+$) (Figures 4G, S6E, and S6F). Together, these findings suggest that treatment selectively enhances B cell migration to, and activation within, the tumor-proximal lymphoid niche.

Identification of HSP70 as the target of anti-melanosome mAbs

Western blot analysis of melanosome lysates containing both surface and internal proteins revealed that all three mAbs

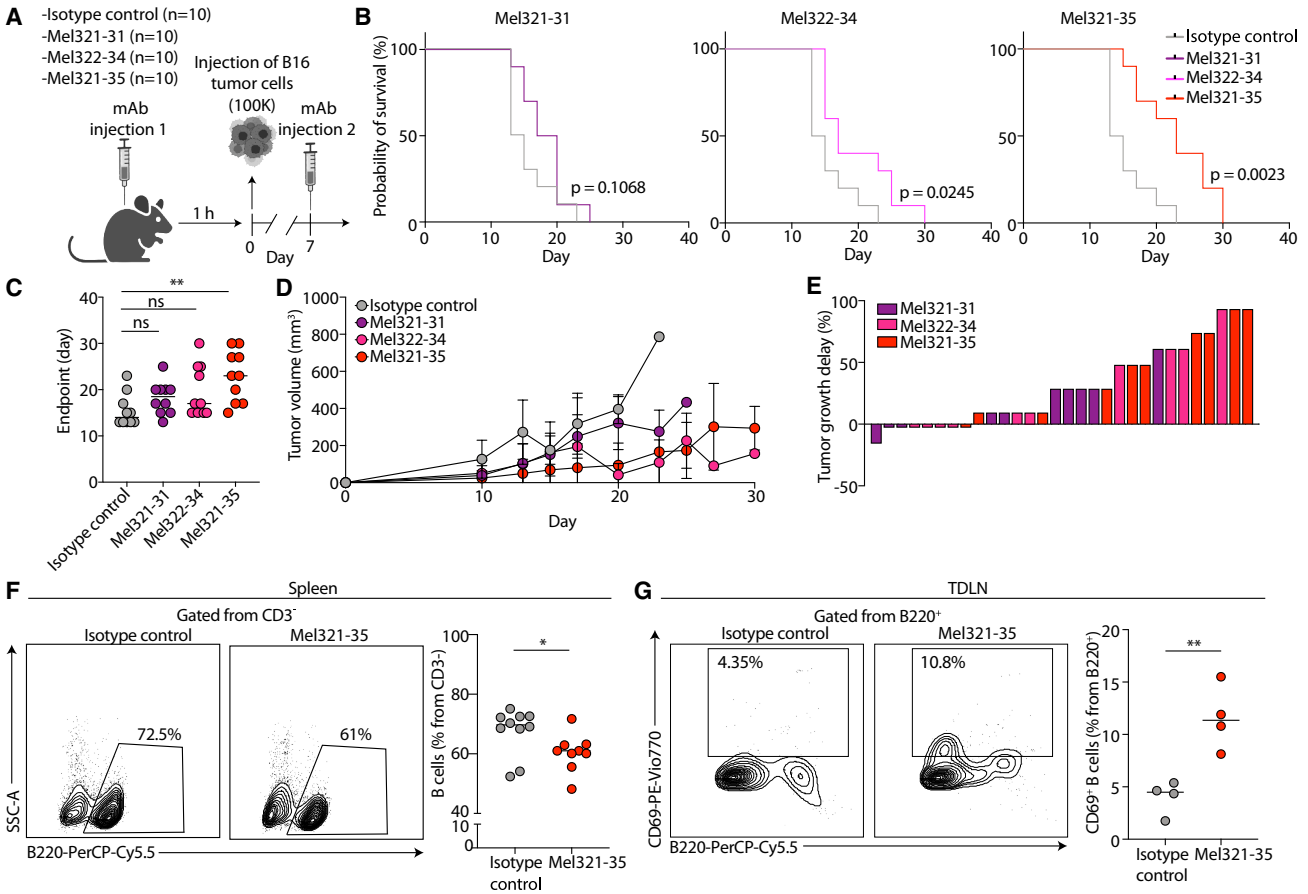

Figure 4. Anti-melanosome mAbs prolong survival in B16-challenged mice

(A) Schematic representation of the passive immunization and tumor challenge strategy. Mice were immunized with 70 μg of the following mAbs Mel321-31, Mel322-34, and Mel321-35 and isotype control, mGO.53. After 1 hour, 100,000 B16 cells were injected subcutaneously into all mice. One week following the mAb and B16 injection, another boost of 35 μg of each mAb was administered to each mouse (n = 10 per group).

(B) Kaplan-Meier survival curves comparing mice treated with mAbs Mel321-31 (purple line, n = 10), Mel322-34 (pink line, n = 10), and Mel321-35 (red line, n = 10) to the isotype control, mGO.53 (gray line, n = 10).

(C) Endpoint day for each mouse. Time to reach the tumor growth limit for individual mice in groups immunized with Mel321-31 (purple circles, n = 10), Mel322-34 (pink circles, n = 10), and Mel321-35 (red circles, n = 10) and isotype control, mGO.53 (gray circles, n = 10).

(D) Tumor volume quantification (in mm^3) over time in mice treated with Mel321-31, Mel322-34, and Mel321-35 and isotype control, mGO.53 (n = 10 per group). Tumor volume was calculated as follows: $V = 0.5 \times \text{length} \times \text{width}^2$. Color code is the same as in (C).

(E) Tumor growth delay (TGD) frequencies for individual mice in the Mel321-31 (purple bars, n = 10), Mel322-34 (pink bars, n = 10), and Mel321-35 (red bars, n = 10) compared to the average of the group of isotype control, mGO.53-immunized mice (n = 10). Calculated as $TGD\% = [(T_{Treated} - T_{Control})/T_{Control}] \times 100$, where $T_{Control}$ is the mean endpoint of the mGO.53-immunized group, and $T_{Treated}$ is the endpoint for each mouse in the Mel321-31-, Mel322-34-, and Mel321-35-immunized groups.

(F) B cell frequency in spleens of treated mice. The left panel shows representative flow cytometry plots of $B220^+$ splenocytes of one Mel321-35- and isotype-control-treated mouse (gated from $CD3^-$; Figure S6), while the right panel shows quantification of the gated population (Mel321-35, n = 8; isotype control, n = 9).

(G) Activated B cell frequency in TDLN of treated mice. The left panel shows representative flow cytometry plots of $B220^+$ $CD69^+$ (gated from $B220^+$; Figure S6) of one Mel321-35- and isotype-control-treated mouse, while the right panel shows quantification of the gated population (Mel321-35, n = 4; isotype control, n = 4).

Graphs (C), (F), and (G) present the mean, and graph (D) presents the mean ± SD, with each symbol representing an individual mouse. Statistical significance was determined using GraphPad Prism by log rank (Mantel-Cox) test in (B), by one-way ANOVA with Tukey's multiple comparisons post-test in (C) and by unpaired two-sided Welch's t test in (F–G). $^*p < 0.05$, $^{**}p < 0.01$; "ns" indicates non-statistically significant differences.

recognized a protein of approximately 70 kDa (Figure 5A). To identify the target, immunoprecipitated proteins were analyzed by liquid chromatography-tandem mass spectrometry (LC-MS/MS), which revealed four highly enriched members of the HSP70 family: HspA1A, HspA1L, HspA5, and HspA8 (Figures 5B, 5C, and S7). ELISA and surface plasmon resonance (SPR) analyses confirmed that Mel321-31, Mel322-34, and Mel321-35 bound to HSP70 family members with measurable affinities (9.87×10^{-9}, 5.52×10^{-9}, 3.1×10^{-9}; Figures 5D and S8). HSP70 proteins are well-known regulators of apoptosis and cell survival and are frequently overexpressed in melanoma and other cancers.[42,43] HSP70 is a potent inhibitor of apoptosis, a

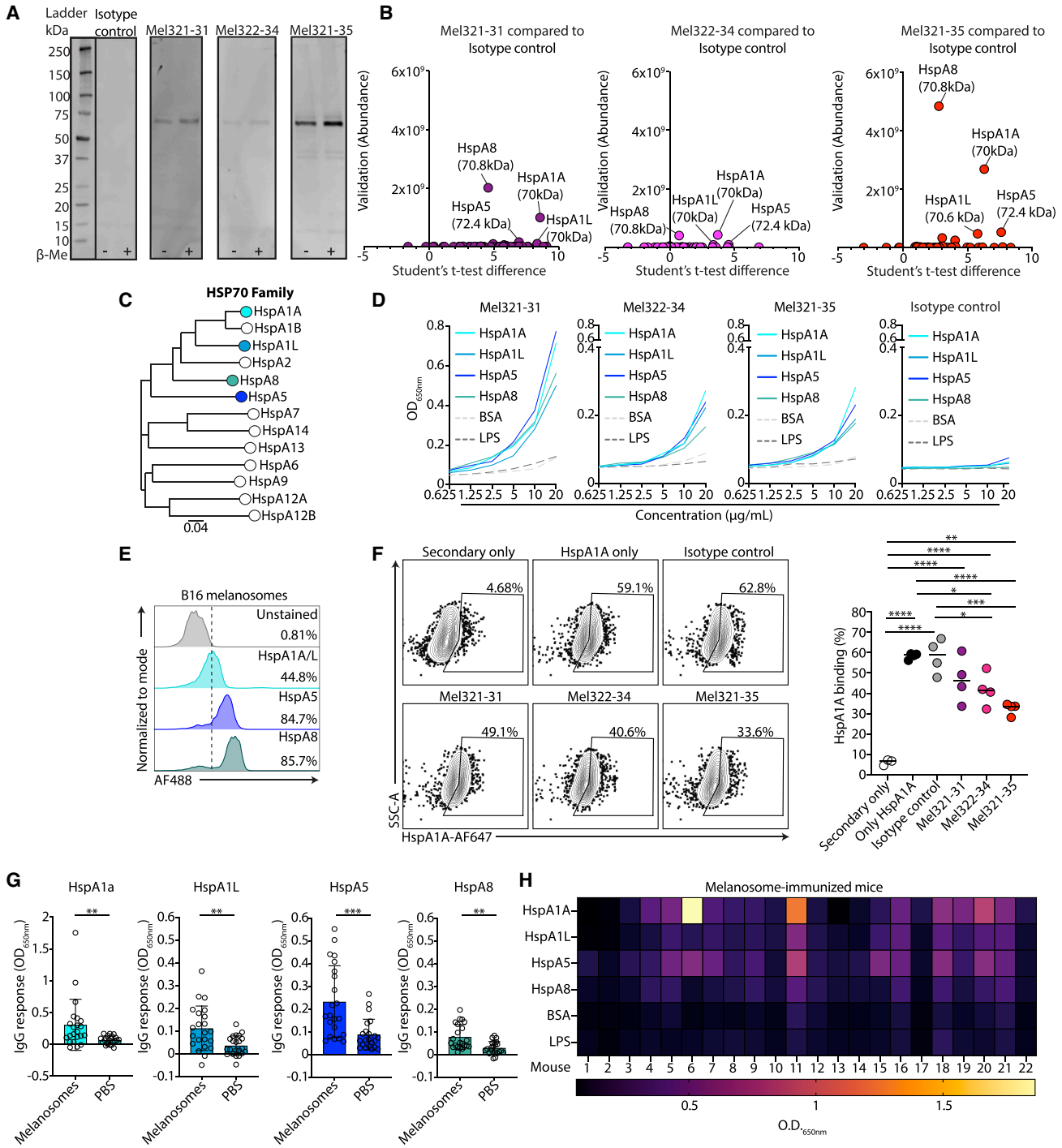

Figure 5. Identification of HSP70 as the target of anti-melanosome mAbs

(A) Western blot analysis showing the binding of mAbs Mel321-31, Mel322-34, and Mel321-35 and the isotype control, mGO.53 to a whole lysate of melanosome proteins; 15 μg of whole lysate was loaded on a protein gel with or without β-mercaptoethanol, followed by incubation with 25 μg/mL of each mAb (Mel321-31, Mel322-34, and Mel321-35 or isotype control, mGO.53) and 1:5,000 anti-mouse secondary antibody; the experiment was repeated three times.

(B) Mass spectrometry analysis showing enriched proteins following immunoprecipitation of proteins from the whole lysate of melanosomes using mAbs Mel321-321 (purple circles, *n* = 4), Mel322-34 (pink circles, *n* = 4), and Mel321-35 (red circles, *n* = 4) compared to isotype control, mGO.53 (*n* = 4). HspA1A, HspA1L, HspA5, and HspA8 and their molecular weight are indicated; the experiment was repeated two times.

(C) Phylogenetic tree showing the mouse HSP70 protein family. The bar at the bottom of the tree provides a scale.

(legend continued on next page)

known activator of the JAK/STAT pathway, and a key suppressor of caspase-3 activity.[44–46] These functional roles align with our earlier findings, in which antibody treatment inhibited cell survival and suppressed IL-6 secretion—further supporting HSP70 as the principal target of the mAbs.

Flow cytometry using commercial antibodies confirmed high surface expression of HspA1A/L (44.8%), HspA5 (84.7%), and HspA8 (85.7%) on B16 murine melanosomes (Figure 5E). Mel322-34 and Mel321-35 significantly inhibited the binding of fluorescently labeled HspA1A to B16 cells, while Mel321-31 showed a non-significant effect (Figure 5F). AlphaFold3 modeling predicted (exhibiting high-confidence, predicted TM-score >0.8) that both mAbs Mel321-31 and Mel322-34 majorly target the nucleotide-binding domain (NBD) across HspA1A, HspA1L, HspA5, and HspA8. Mel321-35, which consistently demonstrated stronger functional activity, exhibited broader specificity, interacting with both the NBD and the substrate-binding domain (SBD) of HspA1A, HspA1L, HspA5, and HspA8 (Figure S9). Finally, we tested the reactivity of sera derived from melanosome-immunized mice against HSP70 family members. As expected, the sera of immunized mice reacted against all four HSP70 family members, in contrast to the sera from PBS-immunized mice, which showed no such reactivity (Figures 5G and 5H). These results indicate that Mel321-31, Mel322-34, and Mel321-35 function as decoy antibodies, binding melanosome-associated HSP70 and blocking its interaction with melanoma cells, thereby disrupting pro-survival signaling.

Anti-HSP70 antibodies correlate with better response to therapy

To assess the relevance of our mAbs to targeting human melanoma, we compared the expression of HSP70 family members in MNT-1 melanoma cell line. All four HSP70 family members were increased in their expression relative to healthy fibroblasts (Figure 6A). HSP70 expression was further confirmed by flow cytometry of purified MNT-1 melanosomes, demonstrating high levels of HspA1A/L (67.6%), HspA5 (64.5%), and HspA8 (66.3%) on the surface of MNT-1 melanosomes (Figure 6B). We next examined whether our mAbs block the survival of MNT-1 cells similarly to what we observed in murine B16 cells. All three mAbs, Mel321-31, Mel322-34, and Mel321-35, induced cell death in MNT-1 (Figure 6C), compared to primary human fibroblasts where no cell death was detected (Figure 6D). Taken together, these results align with prior reports showing strong cross-species conservation of HSP70 family members,[47–49] which likely enables shared recognition by our mAbs.

Lastly, we investigated whether patients with melanoma develop serum antibody responses to HSP70. Of the 38 stage 3 and 4 inoperable metastatic patients with melanoma treated with immune checkpoint inhibitors, 19 achieved a complete response with tumor regression (“Complete Response”), while the remaining 19 showed no response, with continued disease progression (“Progressive Disease”). The Complete Response group exhibited significantly stronger IgG responses to HspA1A and HspA8 compared to the Progressive Disease group (40% and 18.7% increase, respectively, Figure 6E). Furthermore, 100% of the patients in the Complete Response group developed antibodies to HspA1A and HspA5 compared to the Progressive Disease group, where only 68% of the patients developed antibodies to HspA1A and 52% to HspA5 (Figure 6F). These findings suggest a potential association between the presence of anti-HSP70 antibodies and responsiveness to immune checkpoint therapy, indicating a possible functional role for these antibodies in controlling melanoma.

DISCUSSION

Melanoma remains a clinical challenge due to its high metastatic potential, adaptability to diverse microenvironments, and resistance to current therapies.[3,50,51] Recent insights reveal that melanosomes—normally involved in pigment transfer—are repurposed by melanoma cells into potent cancer-promoting agents. Much like viruses, these extracellular vesicles disseminate pro-tumorigenic signals to surrounding cells and reinforce survival pathways, contributing to cancer spread. However, their autocrine role in supporting melanoma cells was not demonstrated. Our study reveals that melanoma-derived melanosomes directly enhance melanoma cell growth, acting as autonomous pro-survival units. Targeted blockade using melanosome decoy antibodies completely abrogated this effect. Remarkably, the antibody treatment not only disrupted melanosome-driven growth and invasion but also induced apoptotic responses. These results uncover a critical self-sustaining mechanism in

(D) Binding of mAbs Mel321-31, Mel322-34, and Mel321-35 and isotype control, mGO.53 to HspA1A, HspA1L, HspA5, HspA8, and two control proteins (BSA and LPS) as measured by ELISA. O.D. values at 650 nm are shown for six antibody dilutions (20, 10, 5, 2.5, 1.25, and 0.625 μg/mL); the experiment was repeated four times.

(E) Histograms showing the expression of HspA1A/L, HspA5, and HspA8 on B16 murine melanosomes, assessed by flow cytometry. The dashed line indicates the threshold for positive staining.

(F) HspA1A binding to B16 cells. Left: representative flow cytometry plots showing the binding frequency of AF647-conjugated HspA1A to B16 cells under different treatment conditions: secondary-only control (streptavidin-AF647, $n = 3$), HspA1A alone ($n = 4$), and AF647-conjugated HspA1A pre-incubated with isotype control mAbs ($n = 4$), Mel321-31 ($n = 4$), Mel322-34 ($n = 4$), and Mel321-35 ($n = 4$). Right: quantification of binding frequencies; the experiment was repeated two times.

(G) Reactivity of IgG antibodies in sera from melanosome-immunized ($n = 22$) and PBS-immunized ($n = 22$) mice as measured by ELISA against HspA1A, HspA1L, HspA5, and HspA8. Raw O.D.650 nm values were obtained after subtracting background binding to BSA; every data point is one mouse; the experiment was repeated two times.

(H) Heatmap representing the values in (G) for each mouse along with reactivity to BSA and LPS. Graph (F) presents the mean, with each symbol representing an individual replicate, and the graphs in (G) present the mean ± SD, with each symbol representing an individual mouse. Statistical significance was determined using GraphPad Prism by one-way ANOVA with Tukey’s multiple comparisons post-test in (F) and by Mann-Whitney U test in (G). $^{*}p < 0.05$, $^{**}p < 0.01$, $^{***}p < 0.001$, $^{****}p < 0.0001$; “ns” indicates non-statistically significant differences.

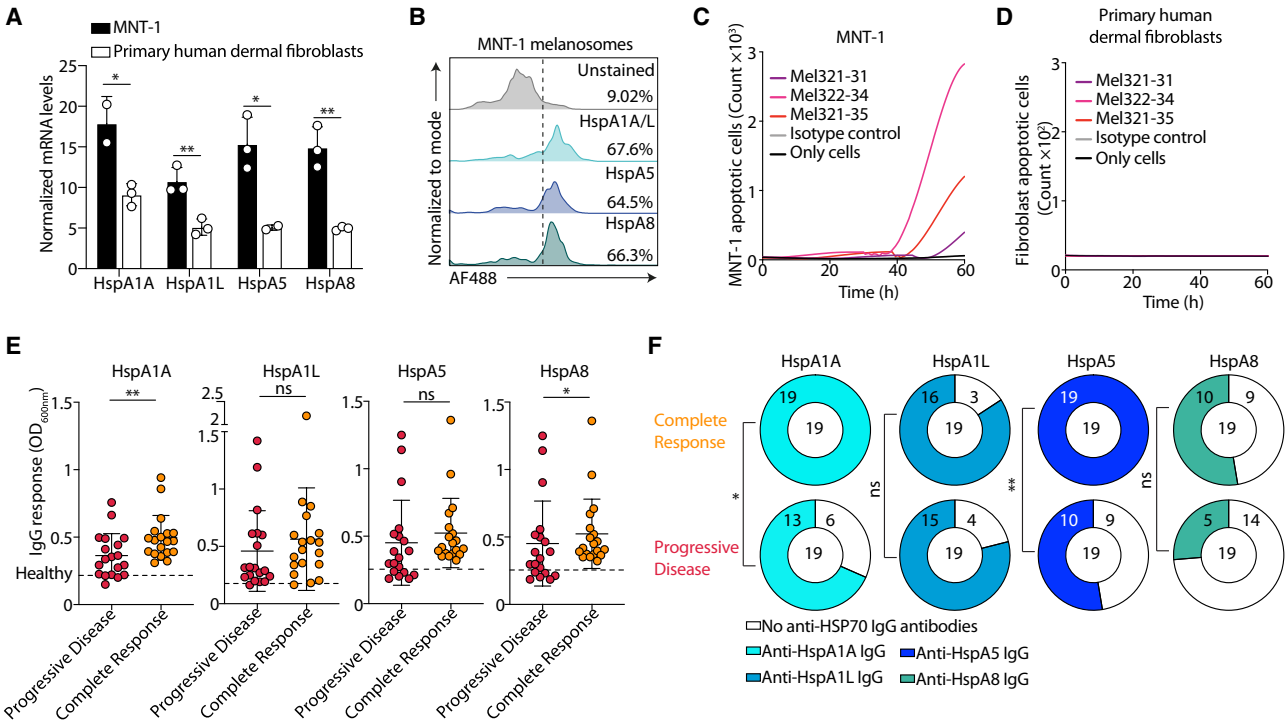

Figure 6. Anti-HSP70 serum response correlates with better response to therapy

(A) Levels of mRNA encoding HSP70 family members (HspA1A, HspA1L, HspA5, and HspA8) in MNT-1 cells and primary human dermal fibroblasts, as measured by real-time PCR (n = 2–3). The results were normalized against the housekeeping gene RPLP0.

(B) Histograms showing the expression of HspA1A/L, HspA5, and HspA8 on MNT-1 human melanosomes, assessed by flow cytometry. The dashed line indicates the threshold for positive staining.

(C and D) Quantification of cell death in MNT-1 cells (C) as well as primary human dermal fibroblasts (D) over 60 h following treatment with mAbs (25 μg/mL, three repeats for each mAb), measured by IncuCyte. No mAb is in black; mGO.53 is an isotype control and is shown as a gray line. The three mAbs Mel321-31, Mel322-34, and Mel321-35 are depicted in purple, magenta, and red, respectively. mAbs were incubated with 15 × 10^3 cells, followed by the addition of a caspase-3/-7 dye; the experiment was repeated two times.

(E) Reactivity of IgG antibodies in sera from patients in the "Progressive Disease" group (red circles, n = 19) and the "Complete Response" group (orange circles, n = 19), assessed by ELISA against HspA1a, HspA1L, HspA5, and HspA8. Raw O.D.600 nm values were obtained after subtracting background binding to BSA. The dashed line represents the mean response of sera from healthy donors (n = 8).

(F) Pie charts illustrating the proportion of patients who developed an IgG response against HspA1a, HspA1L, HspA5, or HspA8. The colored portion represents patients with a detectable IgG response, while the white portion represents those without a response. The top row represents the Complete Response group (n = 19), and the bottom row represents the Progressive Disease group (n = 19). The threshold for a positive response was defined as greater than the mean response of healthy donors (n = 8) + 0.05 O.D.600 nm. Graph (A) presents the mean ± SD, and graph (E) presents the mean ± SD, with each symbol representing an individual patient with melanoma. Statistical significance was determined by unpaired two-tailed Student's t test (A), Mann-Whitney U test (E), and Fisher's exact test (F). *p < 0.05, **p < 0.01; "ns" indicates non-statistically significant differences.

melanoma—a new vulnerability that can be effectively targeted by antibodies.

While melanosomes and melanogenesis have long been associated with tumor progression and metastasis,[32,33,52–54] their capacity to provoke an adaptive immune response has remained unexplored. Unlike other EVs, melanosomes are typically confined to the tumor microenvironment.[28,31] Here, we show that systemic immunization with melanoma-derived melanosomes elicits a robust B and T cell response, leading to prolonged survival and reduced tumor burden in mice. These findings shift the conventional understanding of melanosomes beyond their classical function in pigment transport,[29,55] and pathological function in immune niche deprogramming,[28] positioning them as immunogenic entities and targets for antibodies with direct implications for melanoma therapy.

A key outcome of our study is the identification of HSP70 proteins as central targets of the anti-melanosome antibody response. While previous work—such as that by Komarova et al.—has shown that immunization with HSP70-enriched EVs can reduce tumor growth and improve survival in a B16 melanoma model, those effects were NK-cell-mediated, and the elicited antibodies lacked intrinsic activity.[56] In contrast, our study reveals that melanosome-targeting antibodies induce apoptosis independently of NK cells. Indeed, we observed no changes in NK cell frequencies following melanosome immunization or after passive transfer of anti-melanosome mAbs. Notably, the antibodies act directly upon binding—akin to neutralizing antibodies targeting viral antigens—underscoring a unique autonomous mechanism of action. Another study reports anti-HSP70 mAb isolation by injecting 14-mer HSP70-derived peptides into

mice and generating hybridomas.[57] Similar to what we describe, the generated mAb cmHsp70.1 induced anti-melanoma activity. However, here too, the activity of cmHsp70.1 relied on effector-cell-mediated killing mechanisms.[57] In contrast, we are the first to report that anti-HSP70 mAbs elicited following melanosome immunization mediate melanoma cell killing without any additional effector cells.

HSP70 is highly conserved across a broad range of species, which likely explains the observed cross-reactivity of the antibodies between murine and human melanoma cell lines.[47–49] Furthermore, high HSP70 expression has long been associated with poor prognosis across multiple cancer types, underscoring its clinical relevance in tumor progression.[58] Yet, despite extensive research on its role in oncogenesis, the presence and significance of autoantibodies against HSP70 in patients with cancer have remained largely unexplored. In this study, we uncover a robust autoantibody response to HSP70 in patients with melanoma, which strongly correlates with favorable clinical outcomes and complete response to immune checkpoint blockade therapy. Interestingly, we observed elevated anti-HSP70 antibody levels in complete responders. Notably, anti-melanosome antibody levels did not differ between responders and non-responders (Figure S10), suggesting that the anti-HSP70 response is not a result of general autoreactivity. Instead, these findings raise the possibility that anti-HSP70 antibodies contribute functionally to antitumor immunity, potentially through synergy with other immune cells, as well as directly impairing tumor cell survival. Deeper mechanistic studies investigating how ICI-enhanced $CD8^+$ T cell activity synergizes with antibodies targeting HSP70 are required to determine whether HSP70-targeting antibodies have predictive or therapeutic relevance in melanoma and other HSP70-expressing cancers.

Limitations of the study

Our study establishes a framework for antibody-mediated targeting of melanosomes in melanoma by targeting melanosome-associated HSP70. One limitation is that the observed effects on melanoma cells, both *in vitro* and in mouse models, do not fully recapitulate the heterogeneity of human melanoma disease. As such, the association between elevated anti-HSP70 autoantibody titers and improved patient outcomes is mostly correlative, and whether those antibodies can actively contribute to patient survival remains to be tested in follow-up investigations. Furthermore, the downstream molecular events driving anti-HSP70 autoantibody functions have yet to be fully characterized.

RESOURCE AVAILABILITY

Lead contact

Further information and requests for resources and reagents should be directed to the lead contact, Natalia T. Freund (nfreund@tauex.tau.ac.il).

Materials availability

All requests for materials generated in this study should be directed to the lead contact and will be provided subject to a material transfer agreement in accordance with institutional and patent regulations.

Data and code availability

- RNA sequencing data have been deposited in GEO and are publicly available under accession number GSE319156. Proteomic data have been deposited in PRIDE and are publicly available under accession number PXD074667.
- This paper does not report original code.
- Any additional information required to reanalyze the data reported in this paper is available from the lead contact upon request.

ACKNOWLEDGMENTS

This study is in the memory of Noga Kramer Yakov, who passed away from melanoma at age 39. The study was funded by the Israel Science Foundation (ISF) grants (3136/22) and (638/23) and Binational Science Foundation (BSF) (01031771) to N.T.F. We thank Dr Sterna Germanis-Kaufman for support. N.B.-S. thanks Nilli and Dr Avi Shalev for their support. K.P.'s research is supported in part by a fellowship from the Edmond J. Safra Center for Bioinformatics at Tel-Aviv University. Y.W. is supported by a Melanoma Research Alliance grant (no. 937368), the Rosetrees Trust (no. MYIA\100002), a research grant from Pfizer, and the Lemelbaum family. C.L. acknowledges that this work was funded by the European Research Council (ERC) under the European Union's Horizon 2020 research and innovation program. Views and opinions expressed are however those of the authors only and do not necessarily reflect those of the European Union or the ERCEA. Neither the European Union nor the granting authority can be held responsible for them (C.L., grant agreement no. 726225). This project recieved funding from the European Union Horizon 2020 Marie Sklodowska-Curie grant no. 860635, NEUcrest ITN. We thank Roi Balaban for helping with the *in vivo* experiments. Figures 1A, 2A, and 4A were created using BioRender.com.

AUTHOR CONTRIBUTIONS

N.B.-S. designed and conducted the experiments, analyzed data, prepared figures, and co-wrote the manuscript with N.T.F. S.P. performed mice melanosome immunizations and tumor challenge, which were repeated by N.B.-S. L.A. assisted N.B.-S. with *in vivo* experiments. R.Y. assisted N.B.-S. with ELISA and flow cytometry experiments. P.M., R.P., and S.M. contributed to melanosome production and cell line culturing. D.T.-C. and T.H. contributed to proteomic analysis of the mAb immunoprecipitation experiments. O.M. and M.C. assisted N.B.-S. with mRNA-seq data analysis. K.P. contributed to the statistical analysis. Y.W. and R.S.-F. recruited the patients with melanoma, provided the human sera samples, and applied for the IRB approvals. S.A. contributed conceptually to the idea of immunizing mice with melanosomes. C.L. together with N.B.-S. and N.T.F. participated in the initiation, ideation, and conceptualization of the study. N.T.F. applied for TAU ethics approvals, conceived and supervised the study, analyzed data, prepared figures, and co-wrote the manuscript with N.B.-S.

DECLARATION OF INTERESTS

N.B.-S., N.T.F., S.P., and C.L. are co-inventors on a patent application related to the mAbs described in this study.

STAR★METHODS

Detailed methods are provided in the online version of this paper and include the following:

- KEY RESOURCES TABLE
- EXPERIMENTAL MODEL AND STUDY PARTICIPANT DETAILS
  - Human participants
  - Mice
  - Cell lines and primary cultures
- METHOD DETAILS
  - Mice immunization and tumor model
  - Tissue collection and processing
  - Melanosome purification and characterization
  - ELISA
  - Flow Cytometry
  - Single B cell sorting and sequencing

- Antibody sequence analysis
- Antibody and protein production
- Live-cell imaging
- RNA extraction, library preparation, and sequencing
- Gene Ontology analysis
- Western Blot analysis
- Immunoprecipitation and mass spectrometry
- Amplification and cloning - HSP70
- Transfection, production and protein isolation
- Surface Plasmon Resonance
- Alpha-fold modeling
- RNA isolation and real-time PCR

● QUANTIFICATION AND STATISTICAL ANALYSIS

SUPPLEMENTAL INFORMATION

Supplemental information can be found online at https://doi.org/10.1016/j.celrep.2026.117300.

Received: July 29, 2025
Revised: December 9, 2025
Accepted: April 2, 2026

REFERENCES

1. Saginala, K., Barsouk, A., Aluru, J.S., Rawla, P., and Barsouk, A. (2021). Epidemiology of Melanoma. Med. Sci. *9*, 63.
2. Bell, R.E., and Levy, C. (2011). The three M's: melanoma, microphthalmia-associated transcription factor and microRNA. Pigment Cell Melanoma Res. *24*, 1088–1106.
3. Hodis, E., Watson, I.R., Kryukov, G.V., Arold, S.T., Imielinski, M., Theurillat, J.P., Nickerson, E., Auclair, D., Li, L., Place, C., et al. (2012). A landscape of driver mutations in melanoma. Cell *150*, 251–263.
4. Huang, A.C., and Zappasodi, R. (2022). A decade of checkpoint blockade immunotherapy in melanoma: understanding the molecular basis for immune sensitivity and resistance. Nat. Immunol. *23*, 660–670.
5. Harel, M., Ortenberg, R., Varanasi, S.K., Mangalhara, K.C., Mardamshina, M., Markovits, E., Baruch, E.N., Tripple, V., Arama-Chayoth, M., Greenberg, E., et al. (2019). Proteomics of Melanoma Response to Immunotherapy Reveals Mitochondrial Dependence. Cell *179*, 236–250.e18.
6. Gide, T.N., Wilmott, J.S., Scolyer, R.A., and Long, G.V. (2018). Primary and Acquired Resistance to Immune Checkpoint Inhibitors in Metastatic Melanoma. Clin. Cancer Res. *24*, 1260–1270.
7. Schadendorf, D., Hodi, F.S., Robert, C., Weber, J.S., Margolin, K., Hamid, O., Patt, D., Chen, T.T., Berman, D.M., and Wolchok, J.D. (2015). Pooled Analysis of Long-Term Survival Data From Phase II and Phase III Trials of Ipilimumab in Unresectable or Metastatic Melanoma. J. Clin. Oncol. *33*, 1889–1894.
8. Topalian, S.L., Sznol, M., McDermott, D.F., Kluger, H.M., Carvajal, R.D., Sharfman, W.H., Brahmer, J.R., Lawrence, D.P., Atkins, M.B., Powderly, J.D., et al. (2014). Survival, durable tumor remission, and long-term safety in patients with advanced melanoma receiving nivolumab. J. Clin. Oncol. *32*, 1020–1030.
9. Aya, F., Lanuza-Gracia, P., González-Pérez, A., Bonnal, S., Mancini, E., López-Bigas, N., Arance, A., and Valcárcel, J. (2024). Genomic deletions explain the generation of alternative BRAF isoforms conferring resistance to MAPK inhibitors in melanoma. Cell Rep. *43*, 114048.
10. Haugh, A.M., Salama, A.K.S., and Johnson, D.B. (2021). Advanced Melanoma: Resistance Mechanisms to Current Therapies. Hematol. Oncol. Clin. North Am. *35*, 111–128.
11. Antohe, M., Nedelcu, R.I., Nichita, L., Popp, C.G., Cioplea, M., Brinzea, A., Hodorogea, A., Calinescu, A., Balaban, M., Ion, D.A., et al. (2019). Tumor infiltrating lymphocytes: The regulator of melanoma evolution. Oncol. Lett. *17*, 4155–4161.
12. Kalaora, S., Nagler, A., Wargo, J.A., and Samuels, Y. (2022). Mechanisms of immune activation and regulation: lessons from melanoma. Nat. Rev. Cancer *22*, 195–207.
13. Lee, A.F., Sieling, P.A., and Lee, D.J. (2013). Immune correlates of melanoma survival in adoptive cell therapy. OncoImmunology *2*, e22889.
14. Kravtsov, D.S., Erbe, A.K., Sondel, P.M., and Rakhmilevich, A.L. (2022). Roles of CD4+ T cells as mediators of antitumor immunity. Front. Immunol. *13*, 972021.
15. Micevic, G., Daniels, A., Flem-Karlsen, K., Park, K., Talty, R., McGeary, M., Mirza, H., Blackburn, H.N., Sefik, E., Cheung, J.F., et al. (2023). IL-7R licenses a population of epigenetically poised memory CD8(+) T cells with superior antitumor efficacy that are critical for melanoma memory. Proc. Natl. Acad. Sci. USA *120*, e2304319120.
16. Egbuniwe, I.U., Karagiannis, S.N., Nestle, F.O., and Lacy, K.E. (2015). Revisiting the role of B cells in skin immune surveillance. Trends Immunol. *36*, 102–111.
17. Fridman, W.H., Pagès, F., Sautès-Fridman, C., and Galon, J. (2012). The immune contexture in human tumours: impact on clinical outcome. Nat. Rev. Cancer *12*, 298–306.
18. Dieu-Nosjean, M.C., Goc, J., Giraldo, N.A., Sautès-Fridman, C., and Fridman, W.H. (2014). Tertiary lymphoid structures in cancer and beyond. Trends Immunol. *35*, 571–580.
19. Ladányi, A., Kiss, J., Mohos, A., Somlai, B., Liszkay, G., Gilde, K., Fejös, Z., Gaudi, I., Dobos, J., and Tímár, J. (2011). Prognostic impact of B-cell density in cutaneous melanoma. Cancer Immunol. Immunother. *60*, 1729–1738.
20. Germain, C., Gnjatic, S., Tamzalit, F., Knockaert, S., Remark, R., Goc, J., Lepelley, A., Becht, E., Katsahian, S., Bizouard, G., et al. (2014). Presence of B cells in tertiary lymphoid structures is associated with a protective immunity in patients with lung cancer. Am. J. Respir. Crit. Care Med. *189*, 832–844.
21. Fridman, W.H., Meylan, M., Pupier, G., Calvez, A., Hernandez, I., and Sautès-Fridman, C. (2023). Tertiary lymphoid structures and B cells: An intratumoral immunity cycle. Immunity *56*, 2254–2269.
22. Navon, M., Ben-Shalom, N., Dadiani, M., Mor, M., Yefet, R., Bakalenik-Gavry, M., Chat, D., Balint-Lahat, N., Barshack, I., Tsarfaty, I., et al. (2025). Unique characteristics of autoantibodies targeting MET in patients with breast and lung cancer. JCI Insight *10*, e187392.
23. Helmink, B.A., Reddy, S.M., Gao, J., Zhang, S., Basar, R., Thakur, R., Yizhak, K., Sade-Feldman, M., Blando, J., Han, G., et al. (2020). B cells and tertiary lymphoid structures promote immunotherapy response. Nature *577*, 549–555.
24. Cui, C., Craft, J., and Joshi, N.S. (2023). T follicular helper cells in cancer, tertiary lymphoid structures, and beyond. Semin. Immunol. *69*, 101797.
25. Crescioli, S., Correa, I., Ng, J., Willsmore, Z.N., Laddach, R., Chenoweth, A., Chauhan, J., Di Meo, A., Stewart, A., Kalliolia, E., et al. (2023). B cell profiles, antibody repertoire and reactivity reveal dysregulated responses with autoimmune features in melanoma. Nat. Commun. *14*, 3378.
26. Fässler, M., Diem, S., Mangana, J., Hasan Ali, O., Berner, F., Bomze, D., Ring, S., Niederer, R., Del Carmen Gil Cruz, C., Pérez Shibayama, C.I., et al. (2019). Antibodies as biomarker candidates for response and survival to checkpoint inhibitors in melanoma patients. J. Immunother. Cancer *7*, 50.
27. Stockert, E., Jäger, E., Chen, Y.T., Scanlan, M.J., Gout, I., Karbach, J., Arand, M., Knuth, A., and Old, L.J. (1998). A survey of the humoral immune response of cancer patients to a panel of human tumor antigens. J. Exp. Med. *187*, 1349–1354.
28. Dror, S., Sander, L., Schwartz, H., Sheinboim, D., Barzilai, A., Dishon, Y., Apcher, S., Golan, T., Greenberger, S., Barshack, I., et al. (2016). Melanoma miRNA trafficking controls tumour primary niche formation. Nat. Cell Biol. *18*, 1006–1017.

29. Raposo, G., and Marks, M.S. (2007). Melanosomes–dark organelles enlighten endosomal membrane transport. Nat. Rev. Mol. Cell Biol. *8*, 786–797.

30. Marks, M.S., Theos, A.C., and Raposo, G. (2003). Melanosomes and MHC class II antigen-processing compartments: a tinted view of intracellular trafficking and immunity. Immunol. Res. *27*, 409–426.

31. García-Silva, S., and Peinado, H. (2016). Melanosomes foster a tumour niche by activating CAFs. Nat. Cell Biol. *18*, 911–913.

32. Leichner, G.S., Schweitzer, I., Dror, S., Levin, L., Geva, P., Golan, T., Zaremba, L., Shapira, G., Parikh, R., Shomron, N., et al. (2023). Primary Melanoma miRNA Trafficking Induces Lymphangiogenesis. J. Invest. Dermatol. *143*, 1788–1798.e7.

33. Parikh, R., Parikh, S., Berzin, D., Vaknine, H., Ovadia, S., Likonen, D., Greenberger, S., Scope, A., Elgavish, S., Nevo, Y., et al. (2024). Recycled melanoma-secreted melanosomes regulate tumor-associated macrophage diversification. EMBO J. *43*, 3553–3586.

34. Netanely, D., Leibou, S., Parikh, R., Stern, N., Vaknine, H., Brenner, R., Amar, S., Factor, R.H., Perluk, T., Frand, J., et al. (2021). Classification of node-positive melanomas into prognostic subgroups using keratin, immune, and melanogenesis expression patterns. Oncogene *40*, 1792–1805.

35. Chen, K.G., Valencia, J.C., Lai, B., Zhang, G., Paterson, J.K., Rouzaud, F., Berens, W., Wincovitch, S.M., Garfield, S.H., Leapman, R.D., et al. (2006). Melanosomal sequestration of cytotoxic drugs contributes to the intractability of malignant melanomas. Proc. Natl. Acad. Sci. USA *103*, 9903–9907.

36. Schiaffino, M.V. (2010). Signaling pathways in melanosome biogenesis and pathology. Int. J. Biochem. Cell Biol. *42*, 1094–1104.

37. Briles, E.B., and Kornfeld, S. (1978). Isolation and metastatic properties of detachment variants of B16 melanoma cells. J. Natl. Cancer Inst. *60*, 1217–1222.

38. von Boehmer, L., Liu, C., Ackerman, S., Gitlin, A.D., Wang, Q., Gazumyan, A., and Nussenzweig, M.C. (2016). Sequencing and cloning of antigen-specific antibodies from mouse memory B cells. Nat. Protoc. *11*, 1908–1923.

39. Ben-Shalom, N., Sandbank, E., Abramovitz, L., Hezroni, H., Levine, T., Trachtenberg, E., Fogel, N., Mor, M., Yefet, R., Stoler-Barak, L., et al. (2023). beta2-adrenergic signaling promotes higher-affinity B cells and antibodies. Brain Behav. Immun. *113*, 66–82.

40. Wardemann, H., Yurasov, S., Schaefer, A., Young, J.W., Meffre, E., and Nussenzweig, M.C. (2003). Predominant autoantibody production by early human B cell precursors. Science *301*, 1374–1377.

41. Johnson, D.E., O'Keefe, R.A., and Grandis, J.R. (2018). Targeting the IL-6/JAK/STAT3 signalling axis in cancer. Nat. Rev. Clin. Oncol. *15*, 234–248.

42. Murphy, M.E. (2013). The HSP70 family and cancer. Carcinogenesis *34*, 1181–1188.

43. Kumar, S., Stokes, J., 3rd, Singh, U.P., Scissum Gunn, K., Acharya, A., Manne, U., and Mishra, M. (2016). Targeting Hsp70: A possible therapy for cancer. Cancer Lett. *374*, 156–166.

44. Jäättelä, M., Wissing, D., Kokholm, K., Kallunki, T., and Egeblad, M. (1998). Hsp70 exerts its anti-apoptotic function downstream of caspase-3-like proteases. EMBO J. *17*, 6124–6134.

45. Li, C.Y., Lee, J.S., Ko, Y.G., Kim, J.I., and Seo, J.S. (2000). Heat shock protein 70 inhibits apoptosis downstream of cytochrome c release and upstream of caspase-3 activation. J. Biol. Chem. *275*, 25665–25671.

46. Creagh, E.M., Carmody, R.J., and Cotter, T.G. (2000). Heat shock protein 70 inhibits caspase-dependent and -independent apoptosis in Jurkat T cells. Exp. Cell Res. *257*, 58–66.

47. Daugaard, M., Rohde, M., and Jäättelä, M. (2007). The heat shock protein 70 family: Highly homologous proteins with overlapping and distinct functions. FEBS Lett. *581*, 3702–3710.

48. Hess, K., Oliverio, R., Nguyen, P., Le, D., Ellis, J., Kdeiss, B., Ord, S., Chalkia, D., and Nikolaidis, N. (2018). Concurrent action of purifying selection and gene conversion results in extreme conservation of the major stress-inducible Hsp70 genes in mammals. Sci. Rep. *8*, 5082.

49. Hunt, C., and Calderwood, S. (1990). Characterization and sequence of a mouse hsp70 gene and its expression in mouse cell lines. Gene *87*, 199–204.

50. Shen, K., Song, W., Wang, H., Wang, L., Yang, Y., Hu, Q., Ren, M., Gao, Z., Wang, Q., Zheng, S., et al. (2023). Decoding the metastatic potential and optimal postoperative adjuvant therapy of melanoma based on metastasis score. Cell Death Discov. *9*, 397.

51. Diazzi, S., Tartare-Deckert, S., and Deckert, M. (2023). The mechanical phenotypic plasticity of melanoma cell: an emerging driver of therapy cross-resistance. Oncogenesis *12*, 7.

52. Brożyna, A.A., Jóźwicki, W., Carlson, J.A., and Slominski, A.T. (2013). Melanogenesis affects overall and disease-free survival in patients with stage III and IV melanoma. Hum. Pathol. *44*, 2071–2074.

53. Riaz, N., Havel, J.J., Makarov, V., Desrichard, A., Urba, W.J., Sims, J.S., Hodi, F.S., Martín-Algarra, S., Mandal, R., Sharfman, W.H., et al. (2017). Tumor and Microenvironment Evolution during Immunotherapy with Nivolumab. Cell *171*, 934–949.e16.

54. Slominski, A., Zbytek, B., and Slominski, R. (2009). Inhibitors of melanogenesis increase toxicity of cyclophosphamide and lymphocytes against melanoma cells. Int. J. Cancer *124*, 1470–1477.

55. Sitaram, A., and Marks, M.S. (2012). Mechanisms of protein delivery to melanosomes in pigment cells. Physiology *27*, 85–99.

56. Komarova, E.Y., Suezov, R.V., Nikotina, A.D., Aksenov, N.D., Garaeva, L.A., Shtam, T.A., Zhakhov, A.V., Martynova, M.G., Bystrova, O.A., Istomina, M.S., et al. (2021). Hsp70-containing extracellular vesicles are capable of activating of adaptive immunity in models of mouse melanoma and colon carcinoma. Sci. Rep. *11*, 21314.

57. Stangl, S., Gehrmann, M., Riegger, J., Kuhs, K., Riederer, I., Sievert, W., Hube, K., Mocikat, R., Dressel, R., Kremmer, E., et al. (2011). Targeting membrane heat-shock protein 70 (Hsp70) on tumors by cmHsp70.1 antibody. Proc. Natl. Acad. Sci. USA *108*, 733–738.

58. Zhao, K., Zhou, G., Liu, Y., Zhang, J., Chen, Y., Liu, L., and Zhang, G. (2023). HSP70 Family in Cancer: Signaling Mechanisms and Therapeutic Advances. Biomolecules *13*, 601.

59. Muzellec, B., Teleńczuk, M., Cabeli, V., and Andreux, M. (2023). PyDESeq2: a python package for bulk RNA-seq differential expression analysis. Bioinformatics *39*, btad547.

60. Duvallet, E., Boulpicante, M., Yamazaki, T., Daskalogianni, C., Prado Martins, R., Baconnais, S., Manoury, B., Fahraeus, R., and Apcher, S. (2016). Exosome-driven transfer of tumor-associated Pioneer Translation Products (TA-PTPs) for the MHC class I cross-presentation pathway. OncoImmunology *5*, e1198865.

61. Dobin, A., Davis, C.A., Schlesinger, F., Drenkow, J., Zaleski, C., Jha, S., Batut, P., Chaisson, M., and Gingeras, T.R. (2013). STAR: ultrafast universal RNA-seq aligner. Bioinformatics *29*, 15–21.

62. Anders, S., Pyl, P.T., and Huber, W. (2015). HTSeq–a Python framework to work with high-throughput sequencing data. Bioinformatics *31*, 166–169.

63. Chemla, Y., Itzhaki, O., Melamed, S., Weller, C., Sade, Y., Manich, P., Reshef, K., Xenidis, N., Maliah, A., Levy, G., et al. (2026). HLA export by melanoma cells decoys cytotoxic T cells to promote immune evasion. Cell *189*, 233–251.e29. https://doi.org/10.1016/j.cell.2025.11.020.

64. Freund, N.T., Wang, H., Scharf, L., Nogueira, L., Horwitz, J.A., Bar-On, Y., Golijanin, J., Sievers, S.A., Sok, D., Cai, H., et al. (2017). Coexistence of potent HIV-1 broadly neutralizing antibodies and antibody-sensitive viruses in a viremic controller. Sci. Transl. Med. *9*, eaal2144.

65. Scheid, J.F., Mouquet, H., Feldhahn, N., Walker, B.D., Pereyra, F., Cutrell, E., Seaman, M.S., Mascola, J.R., Wyatt, R.T., Wardemann, H., and Nussenzweig, M.C. (2009). A method for identification of HIV gp140 binding memory B cells in human blood. J. Immunol. Methods *343*, 65–67.

66. Tiller, T., Meffre, E., Yurasov, S., Tsuiji, M., Nussenzweig, M.C., and Wardemann, H. (2008). Efficient generation of monoclonal antibodies from single human B cells by single cell RT-PCR and expression vector cloning. J. Immunol. Methods *329*, 112–124.

67. Polonsky, K., Pupko, T., and Freund, N.T. (2023). Evaluation of the Ability of AlphaFold to Predict the Three-Dimensional Structures of Antibodies and Epitopes. J. Immunol. *211*, 1578–1588. https://doi.org/10.4049/jimmunol.2300150.

68. Cock, P.J.A., Antao, T., Chang, J.T., Chapman, B.A., Cox, C.J., Dalke, A., Friedberg, I., Hamelryck, T., Kauff, F., Wilczynski, B., et al. (2009). Biopython: freely available Python tools for computational molecular biology and bioinformatics. Bioinformatics *25*, 1422–1423.

STAR★METHODS

KEY RESOURCES TABLE

REAGENT or RESOURCE	SOURCE	IDENTIFIER
Antibodies		
Mel321-31 mouse IgG2a	This study	Mel321-31
Mel322-34 mouse IgG2a	This study	Mel322-34
Mel321-35 mouse IgG2a	This study	Mel321-35
Isotype control monoclonal antibody (mGO.53)	This study	mGO.53
Anti-Avi tag monoclonal antibody	Avidity LLC	Cat# AbC; RRID:AB_2810201
HRP-conjugated anti-mouse IgG	Jackson ImmunoResearch	Cat# 115-035-003; RRID:AB_2337946
HRP-conjugated anti-human IgG	Jackson ImmunoResearch	Cat# 109-035-098; RRID:AB_2337595
Precision Protein™ StrepTactin-HRP	Bio-Rad	Cat# 1610380; RRID:AB_2629464
Anti-B220 PerCP-Cy5.5	BioGems	Cat# 07131-70-100; RRID:AB_10854135
Anti-IgM BV421	BioLegend	Cat# 406506; RRID:AB_2561441
Anti-IgG1 BV421	BioLegend	Cat# 406616; RRID:AB_2563105
Anti-GL7 AF647	BioLegend	Cat# 144606; RRID:AB_2563314
Anti-CD95 (FAS) PE-Vio770	Miltenyi Biotec	Cat# 130-120-291; RRID:AB_2660185
Anti-CD4 BV421	BioLegend	Cat# 100438; RRID:AB_2563027
Anti-CD8a FITC	BioLegend	Cat# 100706; RRID:AB_312745
Anti-NK1.1 PE	Miltenyi Biotec	Cat# 130-120-511; RRID:AB_2660188
Anti-CD64 PE-Vio770	Miltenyi Biotec	Cat# 130-119-659; RRID:AB_2660195
Anti-F4/80 APC	Miltenyi Biotec	Cat# 130-116-525; RRID:AB_2660190
Anti-CD69 PE-Vio770	Miltenyi Biotec	Cat# 130-103-977; RRID:AB_2660143
Anti-CD45 BV711	BioLegend	Cat# 103147; RRID:AB_2565858
Anti-HSP70 Alexa Fluor 488	BioLegend	Cat# 648004; RRID:AB_2562980
Anti-GRP78 Alexa Fluor 488	Santa Cruz Biotechnology	Cat# SC-166490; RRID:AB_2262960
Anti-HSC70 Alexa Fluor 488	Santa Cruz Biotechnology	Cat# SC-7298; RRID:AB_2263015
Anti-CD16/CD32	Thermo Fisher Scientific	Cat# 14-0161-85; RRID:AB_469152

(*Continued on next page*)

Continued

REAGENT or RESOURCE	SOURCE	IDENTIFIER
Biological samples		
Sera of patients with melanoma	Sheba Medical Center	IRB SMC-2437-15; This study
Healthy donor sera	Israeli Blood Bank	Approval #0002682-1; This study
Chemicals, peptides, and recombinant proteins		
RIPA buffer	Thermo Fisher Scientific	Cat# 89900
Protein A agarose beads	GE Healthcare	Cat# 17519901
Caspase-3/7 Green Reagent	Sartorius	Cat# 4440
TMB substrate	Abcam	Cat# ab171523
Streptavidin Alexa Fluor 647	BioLegend	Cat# 405237
CaptureSelect™ Biotin Anti-IgG-Fc	Thermo Fisher Scientific	Cat# 7103252100
Ni^{2+}-NTA Agarose	Cytiva (GE Healthcare)	Cat# 17531801
Recombinant HspA1A	This study	See STAR Methods
Recombinant HspA1L	This study	See STAR Methods
Recombinant HspA5	This study	See STAR Methods
Recombinant HspA8	This study	See STAR Methods
Critical commercial assays		
Pierce™ BCA Protein Assay Kit	Thermo Fisher Scientific	Cat# 23225
PureLink™ RNA Mini Kit	Thermo Fisher Scientific	Cat# 12183016
NEBNext® Poly(A) mRNA Magnetic Isolation Module	NEB	Cat# E7490
NEBNext® Ultra™ II Directional RNA Library Prep Kit	NEB	Cat# E7760
ExpiFectamine™ 293 Transfection Kit	Thermo Fisher Scientific	Cat# A14524
Mouse IL-6 Uncoated ELISA Kit	Thermo Fisher Scientific	Cat# 88-7066-88
Multi Tissue Dissociation Kit 1	Miltenyi Biotec	Cat# 130-110-201
BirA Biotin-Protein Ligase Kit	Avidity LLC	Cat# BirA500
Deposited data		
RNA sequencing data	This study	GEO: GSE319156
Proteomics data	This study	PRIDE: PXD074667
Experimental models: Cell lines		
B16-F10 mouse melanoma cells	ATCC	RRID:CVCL_0159
MNT-1 melanoma cells	ATCC	RRID:CVCL_5624
Primary human dermal fibroblasts	This study	See STAR Methods
Expi293F cells	Thermo Fisher Scientific	Cat#A14527; RRID: CVCL_D615
Experimental models: Organisms/strains		
Mouse: C57BL/6J	The Jackson Laboratory	RRID:IMSR_JAX:000664
Oligonucleotides		
qPCR primers	This study	See Table S3
Nested PCR primers (Ig heavy/light chains)	Published sources	See ref. Muzellec et al.[59]; Duvallet et al.[60]
Software and algorithms		
STAR aligner v2.7.10a	Dobin et al.[61]	RRID:SCR_015899
HTSeq v2.0.1	Anders et al.[62]	RRID:SCR_005514
PyDESeq2 v0.4.4	Muzellec et al.[59]	https://github.com/owkin/PyDESeq2
GSEA v4.3.2	Broad Institute	RRID:SCR_003199
GraphPad Prism v9.5.1	GraphPad Software	RRID:SCR_002798
BIAevaluation software	Cytiva	RRID:SCR_014184
AlphaFold3 Server	DeepMind	https://alphafoldserver.com

(*Continued on next page*)

Continued

REAGENT or RESOURCE	SOURCE	IDENTIFIER
PyMOL v3.1	Schrödinger	RRID:SCR_000305
BioRender	BioRender.com	RRID:SCR_018361

EXPERIMENTAL MODEL AND STUDY PARTICIPANT DETAILS

Human participants

Human serum samples were obtained from 38 participants recruited at Sheba Medical Center under clinical study protocol SMC-2437-15, following approval by the Institutional Review Board and in accordance with the Declaration of Helsinki. All participants provided written informed consent prior to inclusion. The study was additionally approved by the Institutional Ethics Committee of Tel Aviv University (protocol 0009876-1). Participant inclusion was based on clinical diagnosis of melanoma. A cohort of healthy donors with no known history of melanoma was recruited as a control group for baseline antibody reactivity comparisons. Healthy donor sera were obtained from the Israeli Blood Bank (approval 0002682-1). Donors were screened for blood type and for antibodies against syphilis (TPHA), HIV I/II, hepatitis B, hepatitis C, human T-lymphotropic virus, and West Nile virus. Sex and age information for human participants are reported in the main text and/or associated figure legends. No analyses stratified by sex or gender were performed, which represents a limitation in the generalizability of the findings.

Mice

All animal experiments were approved by and conducted in accordance with the guidelines of the Institutional Animal Care and Use Committee (IACUC) of Tel Aviv University (permits 01-15-086 and 01-19-003). Female C57BL/6J mice aged 8–12 weeks were obtained from Envigo Laboratories (Jerusalem, Israel). Mice were housed in groups of 3–4 per cage under standard specific-pathogen-free conditions (22 ± 2°C, 12 h light/dark cycle) with *ad libitum* access to food and water. Animals were acclimated for at least 3 weeks prior to experimentation. Experimental groups were matched for age and weight, and animals were allocated to experimental groups prior to treatment. Mice were monitored regularly for health status and signs of distress, and humane endpoints were applied as described below.

Cell lines and primary cultures

Murine B16 melanoma cells and human MNT-1 melanoma cells were maintained in complete DMEM supplemented with 10% fetal bovine serum (FBS), 1% penicillin/streptomycin, and 1% L-glutamine. Cells used for extracellular vesicle production were cultured in vesicle-depleted FBS prepared by ultracentrifugation at 100,000 × g for 2 h. Primary human dermal fibroblasts were isolated as previously described.[33] All cells were cultured at 37°C in a humidified incubator with 5% CO2. All cell lines were tested for mycoplasma contamination and found negative.

METHOD DETAILS

Mice immunization and tumor model

C57BL/6J mice were intravenously injected with 1 or 10 μg of freshly purified melanosomes. For tumor induction, 1×10^5 B16 melanoma cells were injected subcutaneously. Tumor growth was monitored weekly using digital calipers, and tumor volume was calculated as V = 0.5 × L × W ^2, where L represents tumor length and W represents tumor width. For monoclonal antibody (mAb) treatment, 70 μg of each antibody (Mel321-31, Mel322-34, Mel321-35, or isotype control mGO.53) was administered intravenously 1 h prior to tumor cell injection, followed by a booster dose of 35 μg one week later. Mice were euthanized when tumors reached predefined humane endpoints or if signs of distress were observed.

Tissue collection and processing

Blood samples were collected either from the cheek vein of live animals (≤50 μL) or via cardiac puncture following euthanasia. Serum was isolated by clotting and centrifugation and stored at −20°C. Spleens, tumor-draining lymph nodes, and tumors were harvested, mechanically dissociated, and processed into single-cell suspensions. Red blood cells were lysed from spleen samples, and cells were cryopreserved in FBS containing 10% DMSO. Tumors were dissociated using the Multi Tissue Dissociation Kit 1 according to the manufacturer's instructions.

Melanosome purification and characterization

Melanosomes were isolated from B16 cells as previously described.[28,33] Briefly, B16 cells are grown to 60% confluence, media was changed, and they were grown for 5 days. After 5 days, the conditioned media was collected and centrifuged at 300xg for 15 min followed by 1000xg for 30 min. Melanosomes were then pelleted by centrifuging the supernatant at 20,000xg for 70 min. Melanosomes were resuspended in PBS and used as described further. Melanosome trypsinization was made as previously.[33] The

melanosome isolation protocol was calibrated and validated according to MISEV2023 guidelines. Melanosome and exosome size distributions were determined using NanoSight nanoparticle tracking analysis, with melanosomes defined within the 200–500 nm range, and exosomes within 70–100 nm. Differential protein marker analysis was performed by western blot: melanosomes were validated using Tyrosinase, Dopachrome Tautomerase (DCT), and Glycoprotein Non-Metastatic Melanoma Protein B (GPNMB), while small EV populations were characterized using CD63 and α-Enolase. Morphological examination employed both transmission electron microscopy (TEM) and standard electron microscopy (EM), and further particle tracking was achieved via fluorescence labeling and microscopy. Proteomic analyses of EVs utilized mass spectrometry, confirming the separation of exosomes and melanosomes, both of which were classified as EVs per MISEV2023 definitions. Based on this characterization, standardized functional comparison, and validated isolation procedure, all references to melanosomes in the current study designate them as large EVs, in alignment with contemporary guidelines and established methodological literature. Detailed procedures and functional characterization were performed as described in the referenced papers,[28,32,33,60,63] ensuring strict compliance with MISEV2023 protocol recommendations.

ELISA

For the mouse serum ELISA, high-binding 96-well plates were coated with 10 μg/mL of melanosomes or 5 μg/mL of purified protein and incubated overnight at 4°C. Plates were then blocked with blocking buffer for 2 h at room temperature. After blocking, the plates were washed with PBS containing 0.05% Tween 20 (PBST) and incubated with a 1:50 dilution of sera from melanosome-immunized mice for 1 h at room temperature. For the mAbs binding to melanosomes ELISA, 96-well plates were coated with 10 μg/mL of melanosomes or with purified protein and incubated overnight at 4°C. The plates were then washed with PBST and incubated with serial dilutions (as described in Figure legend) of mAbs, for 1 h at room temperature. For the human serum ELISA, high-binding 96-well plates were coated with 5 μg/mL of purified protein or 10 μg/mL of melanosomes and incubated overnight at 4°C. Plates were then blocked with blocking buffer for 2 h at room temperature and incubated with a 1:50 dilution of sera. Following washing with PBST, all plates were incubated with horseradish peroxidase (HRP)-conjugated anti-mouse IgG secondary antibody (0.16 μg/mL) or anti-human IgG secondary antibody (0.16 μg/mL) for 45 min at room temperature, followed by washing. TMB substrate was added, and optical density (OD) was measured at 650 nm. The Mouse IL-6 Uncoated ELISA Kit was performed according to the manufacturer's instructions.

Flow Cytometry

Thawed cells were resuspended in warm RPMI supplemented with 10% FBS, followed by centrifugation at 400*g* for 5 min at 4°C. The cell pellets were resuspended in FACS buffer and blocked with 1 μg/mL of anti-mouse CD16/32 for 15 min at 4°C to prevent non-specific binding. Cells were then stained for 30 min at 4°C with the following anti-mouse antibodies: anti-B220 PerCP-Cy5.5-conjugated (1:100), anti-IgM BV421-conjugated (1:100), anti-IgG1 BV421-conjugated (1:100), anti-GL7 AF647-conjugated (1:100), anti-FAS (CD95) PE-Vio770-conjugated (1:100), anti-CD4 BV421-conjugated (1:100), anti-CD8a FITC-conjugated (1:100), anti-NK1.1 PE-conjugated (1:100), anti-CD64 PE-Vio770-conjugated (1:50), anti-F4/80 APC-conjugated (1:50), anti-CD69 PE-Vio770-conjugated (1:10), anti-CD45 Brilliant Violet 711-conjugated (1:100) antibodies, or anti-human/mouse antibodies: anti-HSP70 Alexa Fluor488-conjugated (1:100), anti-GRP78 Alexa Fluor488-conjugated (1:100), anti-HSC70 Alexa Fluor488-conjugated (1:100). For HspA1A binding analysis by flow cytometry, Streptavidin Alexa Fluor 647 was pre-incubated for 1 h with biotinylated HspA1A. Subsequently, HspA1A (1 μg/mL per sample) was incubated with each monoclonal antibody (50 μg/mL) for 30 min before being added to 10^5 B16 cells. Samples were analyzed using a CytoFLEX S4 flow cytometer.

Single B cell sorting and sequencing

Murine B cells were isolated from the splenocytes of mice using mouse CD19 micro-beads according to the manufacturer's instructions. B cells were mixed with anti-mouse CD16/CD32 (1:100) and then stained with the following anti-mouse antibodies: anti-B220 PerCP-Cy5.5-conjugated (1:100), anti-CD95 (FAS) PE-Vio770-conjugated (1:100), anti-GL7 AF647-conjugated (1:100), IgM FITC-conjugated (1:100) and IgG1 BV421-conjugated (1:100). Single $IgG1^+$ GC B cells were identified ($B220^+$ CD95 $(FAS)^+$ $GL7^+$ IgM^- $IgG1^+$) and were sorted using an Aria III sorter into a 96-well plate containing 4 μL of lysis buffer. Following sorting, the plates were covered and immediately frozen on dry ice and transferred to −80°C until further processing. Lysed cells were thawed on ice for RNA reverse transcription and PCR amplification as described previously.[64–66] Briefly, cDNA was synthesized using random hexamer primers, and SuperScript III Reverse Transcriptase. First round PCR products were used as a template for additional amplification by nested PCR with specific 5′ V and 3′ J primers containing restriction sites as previously described.[65,66] The first round of PCR was carried out as: 98°C for 30 s, 30 cycles of 98°C for 30 s, 50°C (Gamma) or 55°C (Kappa) for 30 s, and 72°C for 30 s. The second round of PCR was carried out under similar conditions, but the annealing temperature was changed to 57°C (Gamma/Kappa) and the number of cycles reduced to 40 instead of 50. Second round PCR products were purified, sequenced, and annotated with IgBLAST.[40]

Antibody sequence analysis

All PCR products were sequenced and analyzed for Ig gene usage, CDR3, and the number of V_H/V_L somatic hyper mutations using IMGT (http://www.imgt.org) IgBLAST (http://www.ncbi.nlm.nih.gov/igblast/) databases. Expanded B cell clonal families were defined by ≥ 2 B cells exhibiting identical V_H J_H genes, and identical V_K J_K genes, displaying ≥75% homology in CDRH3, or in CDRK3 as previously reported.[40]

Antibody and protein production

For mAb cloning, PCR products were purified, digested with the appropriate restriction enzymes, and ligated into the corresponding expression vectors for IgG or IgK. Cloned mAb vectors for the IgG2a heavy chain and Kappa light chain were co-transfected into Expi293F cells at a ratio of 1:3 (H:K/L) using the ExpiFectamine 293 Transfection Kit. Seven days post-transfection, the cell supernatant was collected, filtered (0.22 μm), and incubated with protein A coated agarose beads for 2 h at room temperature. The beads were then loaded onto chromatography columns, washed, and eluted with 50 mM sodium phosphate (pH 3.0) into 1 M Tris-HCl (pH 8.0). Antibodies were buffer exchanged to PBS X1, aliquoted, and stored at −80°C.

Live-cell imaging

B16, MNT1 melanoma cells or primary dermal fibroblasts (15×10^3 cells) were seeded into a 96-well plate with 200 μL of pre-warmed DMEM, supplemented with 10% heat-inactivated FBS. For the direct effect assay, plates were pre-incubated for 30 min, followed by the addition of 25 μg/mL of each mAb directly to the cells. The plates were then immediately incubated and analyzed using the Incucyte SX5 live-cell imaging system. For the external melanosome assay, 25 μg/mL of each mAb was incubated with 5 μg/mL of external melanosomes before being added to B16 cells. To measure apoptosis, Incucyte Caspase-3/7 Green reagent (1:1000) was added to the culture medium, achieving a final concentration of 5 μM for the assay. Brightness and contrast were adjusted equally across all images for display. Samples were monitored using the Incucyte SX5.

RNA extraction, library preparation, and sequencing

Total RNA was extracted and purified from B16 cells following a 24-h treatment with mAbs: Mel321-31, Mel322-34, Mel321-35, and an isotype control (mGO.53). RNA extraction was performed using the PureLink RNA Mini Kit according to the manufacturer's protocol. RNA quality and concentration were assessed using Qubit Fluorometer and Tapestation. For transcriptome analysis, mRNA enrichment was performed using the NEBNext Poly(A) mRNA Magnetic Isolation Module. Library preparation was carried out with the NEBNext Ultra II Directional RNA Library Prep Kit, generating fragments of ∼350 bp (including adaptors). Sequencing was conducted at the Genomics Research Unit, supported by The Alfredo Federico Strauss Center for Computational Neuro-imaging, Faculty of Life Sciences, Tel Aviv University. Libraries were sequenced on the NextSeq2000 platform using a single-end 100 bp read strategy.

Raw reads were aligned to the mouse transcriptome and genome version GRCh39 with annotations from ENSEMBL release 106 using STAR aligner v.2.7.10a.[61] Counts per gene quantification was done using htseq-count v2.01.[62] Genes with a sum of counts below 100 over all samples were filtered out. Gene expression was normalized per one million counts and log-transformed, and differential expression analysis was done with the PyDESeq2 package v 0.4.4[59] with default parameters. Differentially expressed (DE) genes between the treatments were defined by applying a significance threshold of FDR corrected p-value <0.05.

Gene set enrichment analysis (GSEA) was performed using GSEA v.4.3.2 with the GSEA preranked tool. The Molecular Signature Database hallmark gene sets were used to perform pathway enrichment analysis.

Gene Ontology analysis

Differentially expressed genes were analyzed for their involvement in various biological pathways using Gene Ontology (GO) term annotations. The identified apoptosis-associated pathways include: GO:0006915, GO:0001783, GO:0042981, GO:0097192, GO:0043065, GO:0070059, GO:0006919, GO:0008630, GO:0008635, GO:0044346, GO:0070242, GO:1902262, GO:0097190, GO:1901030, GO:0008637, GO:0043524, GO:0043066, GO:0006919, GO:2001235, GO:0002904, GO:0044336, GO:0044337, GO:1902255, GO:2001243.

Western Blot analysis

Fresh melanosomes were lysed in radioimmunoprecipitation assay (RIPA) buffer and incubated on a rotator at 4°C for 1 h. Lysates were centrifuged at 12,000 g for 15 min at 4°C, and protein concentration was determined using the Pierce BCA Protein Assay Kit. 30 μg of each lysate was mixed with SDS reducing sample buffer, boiled for 5 min, separated by SDS-PAGE, and transferred onto a Trans-Blot Turbo nitrocellulose membrane. Membranes were blocked with 3% BSA in PBS (X1) for 1 h at room temperature and incubated with specific primary antibodies (Mel321-31, Mel322-34, Mel321-35, and mGO.53) overnight at 4°C with gentle agitation. For HSP70 protein detection, 1 μg of each purified protein was mixed with SDS reducing sample buffer, boiled for 5 min, separated by SDS-PAGE, and transferred onto a Trans-Blot Turbo nitrocellulose membrane. Following transfer, membranes were blocked with 3% BSA in PBS (X1) for 1 h at room temperature and incubated overnight at 4°C with gentle agitation with an anti-Avi tag monoclonal antibody. Detection was performed using an HRP-conjugated anti-mouse IgG secondary antibody, Precision Protein StrepTactin-HRP Conjugate (1:5000) and ECL reagent.

Immunoprecipitation and mass spectrometry

The samples were cleaved with trypsin and analyzed by LC-MSMS using the Q Exactive HF mass spectrometer, The data was analyzed with proteome Discoverer 2.4 software and the Sequest search engine against the specific database and a decoy database (in order to determine the false discovery rate, FDR). All the identified peptides were filtered with high confidence −1% FDR threshold. (*FDR = is the estimated fraction of false positives in a list of peptides). Quantitation was done by calculating the peak area of each

peptide. The abundance of the protein is the sum of all associated peptide group abundances. *t* test analysis between each group and the control was done using the Perseus software. p value < 0.05. Supplementary file 1: Proteins with a $\log_2$ fold change (FC) > 2 compared to the isotype control were highlighted in yellow in the Difference column. The Gene Name column includes color-coded annotations corresponding to different statistical tests applied. Differentially expressed proteins specific to the experimental groups, relative to the control (mGO.53, isotype control), are organized in separate tabs: one tab includes proteins consistently enriched across all three sample groups, while additional tabs categorize proteins specific to one or two experimental groups.

Amplification and cloning - HSP70

To produce HSP70, 0.1×10^6 B16 cells were seeded in a 24-well plate and incubated for 24 h. Total RNA was extracted using the PureLink RNA Mini Kit according to the manufacturer's protocol. cDNA synthesis was performed using the qScript cDNA Synthesis Kit, and cDNA concentration was measured with Qubit dsDNA High-Sensitivity Assay Kit. Amplification of HspA1A, HspA1L, HspA5, and HspA8 was carried out using the primers listed in Table S2 and the KAPA HiFi HotStart ReadyMix. The PCR reaction consisted of 12.5 μL KAPA HiFi HotStart ReadyMix, 0.3 μM forward primer, 0.3 μM reverse primer, and 1 ng of template DNA, adjusted to 25 μL with DNase/RNase-free water. The thermocycling conditions were: 95°C for 3 min (initial denaturation), 30 cycles of 98°C for 20 s, 60°C for 15 s, and 72°C for 120 s, Final extension at 72°C for 2 min. PCR products were purified, digested with restriction enzymes, and ligated into the pcDNA 3.1 (+) mammalian expression vector. Each construct included an N-terminal signal peptide (MKAPAVLAPGILVLLFTLVQRSNG) and two C-terminal tags: a hexahistidine tag (His-tag, HHHHHHHH) and a site-specific biotinylation tag (AviTag, GLNDIFEAQKIEWHE). Phylogenetic trees were constructed based on the sequences using Geneious Prime 2024.0.

Transfection, production and protein isolation

Mammalian expression vectors containing the appropriate protein insert were transfected into Expi293F cells using the ExpiFectamine 293 Transfection Kit. For antibody expression, a 1:3 heavy-to-light chain ratio was used. Seven days post-transfection, the cell supernatant was collected, filtered (0.22 μm), and incubated with Ni^{2+}-NTA or Protein A-coated agarose beads (GE Life Sciences) for 2 h at room temperature (RT). Proteins were eluted using 250 mM imidazole, buffer-exchanged into PBS (1×), aliquoted, and stored at −80°C. Antibodies were eluted using 50 mM sodium phosphate (pH 3.0) into 1 M Tris-HCl (pH 8.0) and underwent a similar purification process. When required, proteins were biotinylated using the BirA biotin-protein ligase kit according to the manufacturer's protocol.

Surface Plasmon Resonance

All Biacore experiments were performed at 25°C with a Biacore T200 instrument. On a Series S Sensor Chip SA (GE Healthcare), 10 μg/mL CaptureSelect Biotin Anti-IgG-Fc (Multi-species) conjugate was immobilized at a flow rate of 10 μL/min for 600 s. Over the chip-bound CaptureSelect, each mAb sample (Mel321-31, Mel322-34, Mel321-35, and isotype control mGO.53) at 1 μg/mL was injected at a flow rate of 10 μL/min for 600 s at five sequential concentrations (31.25, 62.5, 125, 250, and 1000 nM). After each cycle, the chip was regenerated with 0.1 M glycine, pH 2, at a flow rate of 30 μL/min for 90 s. Each antibody was tested in duplicate. Samples were diluted in HBS-EP buffer (10 mM HEPES, 150 mM NaCl, 3 mM EDTA, 0.05% Tween 20, pH 7.4). Sensorgrams were generated for each sample, and the curves were fitted to a 1:1 binding model in the BIAevaluation software using nonlinear regression. KD was calculated as the ratio of the dissociation (Kd) and association (Ka) rate constants, KD = Kd/Ka.

Alpha-fold modeling

The protein complex and interactions formed between the mAbs (Mel321-31, Mel322-34, Mel321-35) and the proteins (HspA1A, HspA1L, HspA5 and HspA8) were modeled using the AlphaFold3 Server[67] (https://alphafoldserver.com). Antibody-binding contact residues on HspA1A, HspA1L, HspA5, and HSPa8 were extracted using a Python[68] script (Supplementary file 1), applying a 5.0 Å distance cutoff. The extracted contact residues were then annotated using PyMOL 3.1. Model_0.cif was selected as the default structure. Only structures exhibited a confidence score (predicted TM-score) of pTM >0.8 were used.

RNA isolation and real-time PCR

RNA was isolated using PureLink RNA according to the manufacturer's instructions. This was followed by cDNA synthesis using a qScript synthesis kit, with the cDNA concentration assessed by NanoDrop. The qPCR mix was prepared using SYBR green with the primers described in Table S3, Relative transcript expression was calculated using the ddCt method and all transcripts were normalized RPLP0.

QUANTIFICATION AND STATISTICAL ANALYSIS

All statistical analyses were performed using GraphPad Prism (version 9.5.1; GraphPad Software Inc., San Diego, CA, USA). Data were first assessed for normality using the Shapiro–Wilk test (for small sample sizes) or the D'Agostino–Pearson omnibus (K2) test (for larger datasets). For comparisons between two groups, we used: Unpaired two-tailed Student's *t* test for normally distributed data with equal variances. Unpaired two-tailed Welch's *t* test for normally distributed data with unequal variances. Mann–Whitney U

test for non-normally distributed data. For comparisons among three or more groups, we used: One-way ANOVA, followed by Tukey's multiple comparisons test for normally distributed data. Kruskal–Wallis test, followed by Dunn's multiple comparisons test, for non-normally distributed data. For repeated measures data, we used: Repeated-measures one-way ANOVA, followed by Tukey's multiple comparisons test. For Kaplan–Meier survival curves, we used the log rank (Mantel–Cox) test to compare survival distributions between groups. For categorical data, we used: Fisher's exact test for small sample sizes. All p-values were two-tailed, with $p < 0.05$ considered statistically significant. Adjustments for multiple comparisons were made using Tukey's or Dunn's post hoc tests, as appropriate. Data Presentation: Quantitative data are reported as mean ± standard deviation (s.d.) unless otherwise stated. Boxplots display the median, interquartile range (IQR), and whiskers extending to 1.5× IQR. Individual data points are plotted where possible.